# LINE WIDTH PARAMETERS AND CENTER FREQUENCY SHIFTS IN THE ROTATIONAL SPECTRUM OF METHYL CYANIDE

DISSERTATION

Presented to the Graduate Council of the
North Texas State University in Partial
Fulfillment of the Requirements

For the Degree of

DOCTOR OF PHILOSOPHY

By

David L. Swindle, B.S., M.S.
Denton, Texas
May, 1978

Swindle, David L., Line Width Parameters and Center Frequency Shifts in the Rotational Spectrum of Methyl Cyanide. Doctor of Philosophy (Molecular Physics), May, 1979, 96 pp., 3 tables, bibliography, 40 titles.

Measurement of the line width parameters of a molecule is of interest because collision diameters can be calculated from them. This gives an effective size of the molecule when it is involved in interactions with other molecules. Further, specific types of interactions can be inferred from detailed information about the dependence of the line width upon pressure. In this paper, an experiment for measuring line width parameters for methyl cyanide is described and the results of the experiment are analyzed.

The rotational transitions of methyl cyanide are characterized by very involved quadrupole hyperfine components which overlap significantly as the lines broaden. A model is developed which takes into account modulation broadening, Doppler broadening, and overlap broadening, in an attempt to extract the pressure-broadening parameter from these extraneous effects. This model is relatively successful in allowing insight into the various mechanisms which affect the absorption line shape, and offers hope for analysis of other molecular systems whose rotational

spectra are complicated by overlapping hyperfine structures.

This same model also aids in the analysis of the shift in center frequency of the absorption line. This is also a collision-induced process, and is complicated by the interaction of the overlapping lines present in the spectrum of methyl cyanide.

This investigation was successful in obtaining precise values for the line width parameter for the J-J' = 0-1, J-J'= 1-2, and J-J' = 2-3 transitions of methyl cyanide which agree with experimental values of other researchers where available. It was found that standing waves were the dominant effect in the measurement of center frequency shift.

TABLE OF CONTENTS

TABLE OF CONTENTS (Cont.)

## LIST OF TABLES

## LIST OF ILLUSTRATIONS

LIST OF ILLUSTRATIONS (Cont.)

# CHAPTER I

## INTRODUCTION

H. A. Lorentz[1] and P. Debye[2] laid the early foundations for the theory of molecular collisions in the early 1900's. Weisskopf[3] followed with a more comprehensive description of the origin of spectral lines in the microwave region, but the spark gap radio-frequency generators at that time were scarcely reliable enough to observe the strongest absorption lines, much less to study them in detail. It remained for the technological thrust of World War II with the development of radar to provide stable sources of microwave radiation. Accompanying this boon to the experimentalist were the theoretical developments of Gordy,[4] Van Vleck and Weisskopf,[5] and P. W. Anderson.[6] Anderson's milestone publication has provided a basis for the later impact theories which, along with Anderson's theory, provide the current theoretical description of molecular collisions. These contributions by Murphy and Boggs,[7] Tsao and Curnutte,[8] and Frost[9] are examined with varying degrees of detail in the discussion which follows.

Widespread manufacture of klystrons, magnetrons, and traveling wave tubes provided the needed development of stable and reliable sources of microwave radiation. The area of spectroscopy under investigation requires a very

stable, easily controlled source of low-power microwave radiation. The reflex klystron generally fills this need under most circumstances, and various models of these klystrons were used exclusively in this investigation.

Two principal requirements must be fulfilled if a molecule is to be suitable for microwave probing. They are,

1. The molecule must possess a large electric dipole moment (on the order of one debye* or larger) since the intensity of the absorption is proportional to $|\mu_{ij}|^2$, where $\mu_{ij}$ is the dipole moment matrix element connecting two rotational states.

2. The molecule must possess a vapor pressure large enough to yield an observable microwave spectrum.

Early microwave probing has yielded significant advances in the measurement of molecular bonding angles, interatomic bond distances, atomic masses, nuclear spin, molecular dipole and quadrupole moments, and nuclear quadrupole moments. More recently, interest has focused around analysis of inter-molecular collision mechanisms. One application of this analysis points to radio astronomy, where the discovery of assorted polyatomic organic molecules has raised some inquiries as to the specific nature of molecular collisions in a low-density environment. If quantitative information could be drawn from spectral line shapes as

* One debye = $10^{-18}$ statcoulomb-cm

observed by the radio astronomer, the interstellar environment could be better analyzed. One of the organic molecules, methyl cyanide, is the subject of this investigation.[10] Three others, formic acid, ammonia, and formaldehyde, have been investigated and reported by Venkatachar and Roberts.[11,12,13]

Methyl cyanide is a symmetric top-type molecule possessing three-fold rotational symmetry about the C-C≡N bond axis. The indicated interatomic distances and bond angles shown in Figure 1 were determined by microwave spectroscopic analysis utilizing isotopic substitution.[14] The electric dipole moment of methyl cyanide has been determined using a Stark effect method, and its reported values are 3.92± 0.06 debye[15] and 3.97 debye.[16]

The rotational constants and centrifugal distortion constants have been measured[17] and are tabulated in Table I.

The nitrogen nucleus in methyl cyanide has an intrinsic spin of I = 1, and this gives rise to an appreciable electric quadrupole moment. It can be shown both classically and quantum mechanically that there arises an interaction between this nuclear quadrupole moment and the electron cloud, which results in a perturbation of the rotational energy levels. This perturbation is observed as hyperfine splitting of the spectral lines. These so-called quadrupole components of the spectrum will be seen to be a major

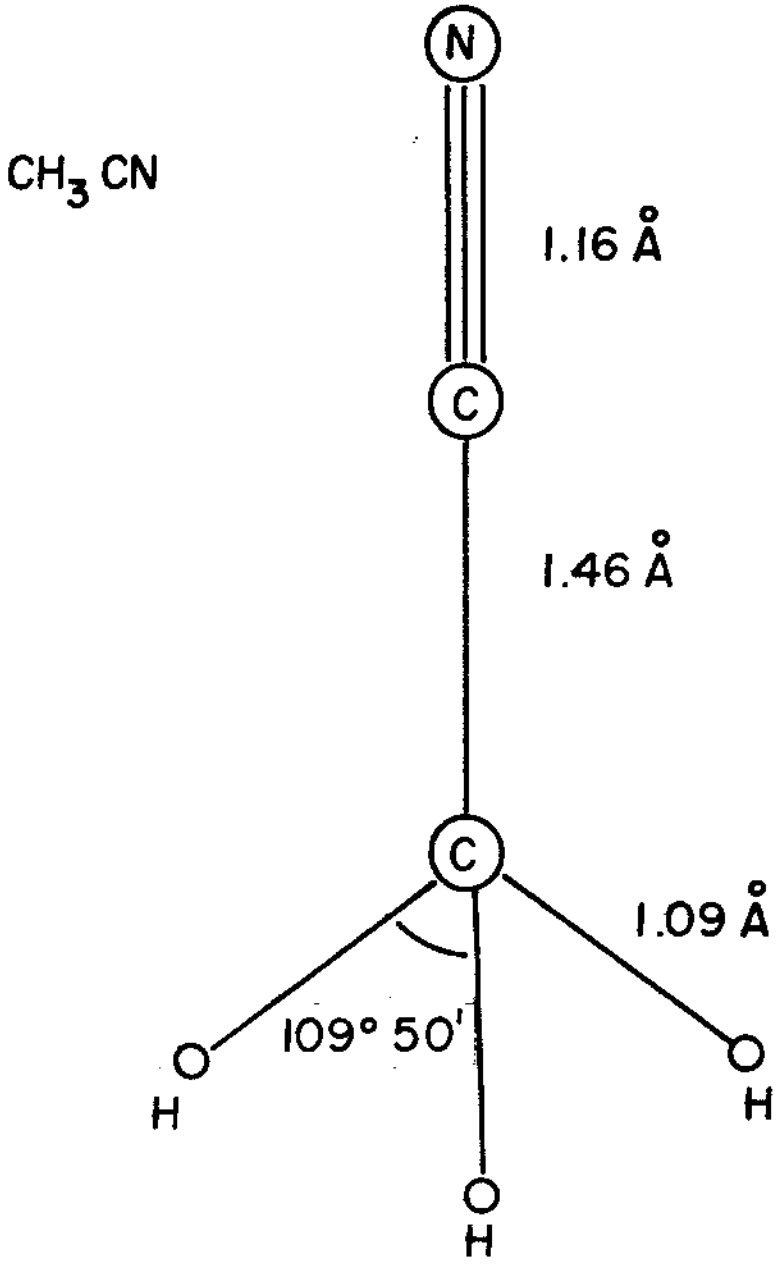


Fig. 1--Schematic representation of the molecular structure of $CH_3CN$ as determined by microwave probing, ref. 14.

TABLE I

MOLECULAR CONSTANTS OF METHYL CYANIDE FROM HIGH-RESOLUTION SPECTROSCOPY[17]

| Property | Symbol | Value (Khz) |
|---|---|---|
| Rotational Constant | B | 9,198,899.299 |
| Centrifugal Distortion | $D_{JK}$ | 177.417 |
| Quadrupole Coupling Strength | eqQ | -4,255.34 |

complicating factor when attempting to analyze spectral characteristics. These components lie so close to the transitions of interest that the idealized line shape cannot be employed.

This investigation began with measuring the half width at half maximum and the center frequency shift of several spectral lines of methyl cyanide. These measurements were made on those hyperfine components that were resolvable over a pressure range of 0.1 millitorr to about 30 millitorr. As the complexities of the spectra involving overlapping lines became evident, it was necessary to incorporate into a mathematical model all effects which contribute to the width of the spectral lines. This model made it possible to analyze pressure broadening and center frequency shifts of spectral lines whose overlapping hyperfine components are very involved. As is explained in following chapters, the variation of half width with pressure is a characteristic parameter of a molecular system, and was used in this investigation to calculate collision diameters which are indications of specific types of molecular interaction mechanisms. The high resolution of the spectrograph utilized in this investigation allowed the determination of collision diameters corresponding to individual hyperfine lines, which were

found to be consistent with previous results for measurements on the unresolved envelope of hyperfine components.

The spectrograph mentioned above has been described by Roberts[18] and is shown schematically in Figure 2. It basically consists of a regulated high voltage supply for the klystron, two coiled wave guides to serve as absorption cells, a phase-sensitive detection system, and a display system. Since the reflex klystron is a voltage-controlled device, frequency modulation was readily obtained through control of the voltage supplied to the klystron. One of the absorption cells was used as a reference, while the other was monitored under various pressure and temperature ranges. The gas handling system was exterior to the spectrograph and allowed close control of the pressure within the absorption cells.

In Chapter III, a brief presentation of some line width theories concerning spectral lines is given. Particular attention is directed at the problems encountered when dealing with overlapping lines. Chapter IV contains further discussion of the spectrograph introduced above, Chapter V contains the quantitative results of this investigation as well as analysis of these results, and Chapter VI is the conclusion to the paper. In the following chapter, a discussion of the shape and width of spectral lines is given.

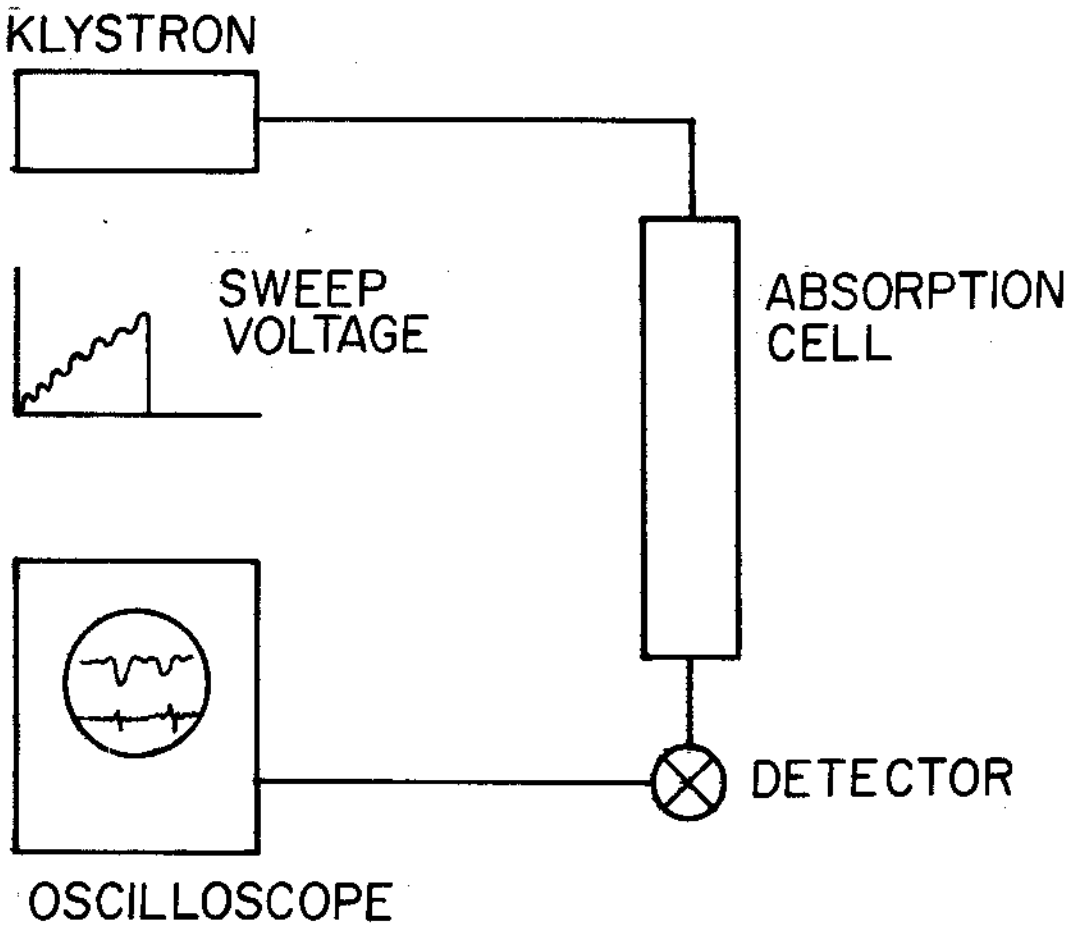


Fig. 2--Brief schematic of the spectrograph used for line width measurement.

# CHAPTER II

## SPECTRAL LINE SHAPES

A study of spectral line widths and shapes is undertaken because they carry information about collision interaction mechanisms, molecular state lifetimes, and other items of interest. A spectral line may be characterized by the following properties:

1. the centroid corresponding to the center frequency;

2. the height (or depth) of the absorption profile, i.e., the relative intensity; and

3. the half width of the absorption or emission profile at half the maximum height.

The great majority of molecular rotational transitions are characterized by an energy whose corresponding frequency lies in the microwave region of the electromagnetic spectrum. This region is generally defined to be from 100 megahertz to 300 gigahertz. Although a small number of rotational transitions have been observed to lie in the infrared region, and conversely some vibrational transitions such as the inversion of ammonia have been observed in the microwave region, the transitions of the molecule here under consideration are treated as purely rotational.

Much theoretical work has been done in an attempt to explain the experimental data for molecules which absorb and emit radiation. The quantization of these energy levels derives from fundamental quantum mechanics; hence a discrete spectrum is expected. Less intuitive is an explanation of the finite width of these lines; that is, a spread in the frequency absorbed and emitted by a quantized system. The sources of this spread are

1. natural line width,
2. absorption cell wall broadening,
3. saturation broadening,
4. pressure broadening,
5. modulation broadening,
6. Doppler effect broadening, and
7. overlapping line distortion.

## Natural Line Width

The natural line width arises due to zero point vibrations in the electromagnetic field, or classically, from self-damping of the oscillator. This width, $\Delta\nu$, has been shown for most molecular systems to be on the order of a few tenths of a hertz or less, i.e.,[19]

$$\Delta\nu = \frac{32\ \pi^3\ \nu^3}{3hc^3}\ |\mu|^2\ , \qquad (1)$$

where h is Planck's constant, $\nu$ is the frequency of transition

and $\mu$ is the magnitude of the dipole moment of the molecule.

## Cell Wall Broadening

Absorption cell wall broadening depends on the size of the cell used since it arises from collisons of the molecule with the walls of the absorption cell. It can be calculated from the geometric factors of the cell and so can be kept small by judicious choice of dimensions. In any case, it contributes only a constant factor to the width at any pressure and so is unimportant in the determination of the line width parameter, $\Delta\nu_p$.

## Saturation Broadening

Saturation broadening occurs when the thermal equilibrium of the gas is upset due to an excessive input of microwave power. This prevents the excited state from relaxing, with a corresponding emission of radiation. A maximum power absorption for molecules has been calculated by Gordy[4], and effects of saturation broadening must be minimized. It has been experimentally observed that saturation occurs at power levels of one milliwatt/cm$^2$. Power levels in this investigation were kept significantly below this figure.

## Pressure Broadening

In 1906, Lorentz[1] treated the molecules of gas in a radiation field as radiating dipoles randomly interrupted

by collisions with other molecules. By performing a Fourier analysis of the radiation wave train, a theory of pressure broadening was deduced. This theory produced good results in the microwave region. A similar idea of rotating dipoles was followed by Debye[2], with the difference that the molecules were distributed according to the Boltzmann law. These collisions were assumed to be adiabatic, resulting only in a relative phase change in the radiation. This approach was continued by Wigner and Weisskopf[20], who derived an expression for the expected shape of a spectral line to be

$$f(\nu,\nu_o) = \frac{\nu}{\pi\nu_o}\left\{\frac{\Delta\nu}{(\nu-\nu_o)^2+(\Delta\nu)^2} + \frac{\Delta\nu}{(\nu+\nu_o)^2+(\Delta\nu)^2}\right\} \qquad (2)$$

where $\nu_o$ is the center frequency, $\Delta\nu$ is the half width at half maximum, and $\nu$ is the independent variable. The second term is negligible near resonance and is usually ignored. This function is a form usually referred to as Lorentzian and is widely used for calculations of theoretical line shapes.

$\Delta\nu$ is the half width due to collisions, usually referred to as the pressure-broadened half width. Since collisions interrupt the radiation or emission process, $\Delta\nu$ can be related to the mean time between collisions $\tau$ by[5]

$$\Delta\nu = \frac{1}{2\pi\tau}. \qquad (3)$$

It is useful to define a collisional cross section $\sigma$

$$\sigma = \frac{1}{n\bar{v}\tau}, \tag{4}$$

where $\bar{v}$ is the mean relative impact velocity and n is the density of molecules in the system. Combining equations (3) and (4) gives

$$\Delta\nu = \frac{n\bar{v}\sigma}{2\pi} . \tag{5}$$

This makes explicit the linear relationship between $\Delta\nu$ and the density of the system. Since the number density of molecules is directly proportional to the pressure of the system, the line width parameter $\Delta\nu_p$ is the slope of the line obtained when plotting $\Delta\nu$ vs. pressure, and is given by

$$\Delta\nu_p = \frac{d(\Delta\nu)}{dn} = \frac{\bar{v}\sigma}{2\pi} . \tag{6}$$

This results from the Van Vleck-Weisskopf theory[5], but is incomplete in that $\Delta\nu$ or $\Delta\nu_p$ is merely an empirical parameter. As will be seen later, the theory of Anderson[6] incorporates $\Delta\nu$ as a directly calculable quantity.

## Modulation Broadening

When a periodically varying voltage is applied to the repeller of a reflex klystron, the radiation output is frequency modulated. The parameters depend on the specific

response sensitivity of the klystron to the applied voltage. This frequency modulation allows a step-by-step sampling of the slope of the pressure-broadened absorption line and so allows the use of ac amplification after detection. This sampling also corresponds to a frequency derivative of the line shape. This was predicted by Karplus[21] and later shown experimentally by Rhinehart *et al.*[22] Further study has been done on higher order derivatives by Netterfield *et al.*[23] If the post-detection amplification is done with a very narrow band-pass amplifier and modulation is effected by a periodic voltage of frequency f/n, where n is an integer and f is the center frequency of the band-pass amplifier, the output of the amplifier will correspond to the $n^{th}$ derivative of the absorption line shape.

The Lorentzian line shape is an integral part of collisional theories, and its validity has been demonstrated by Murphy and Boggs.[7] As has been discussed earlier, the half power points of the absorption lines must be determined with precision. To facilitate the precise location of the resonance's half power points, derivatives are taken electronically and displayed on an oscilloscope trace or chart recorder trace. Figure 3 shows the Lorentzian line shape and its first four derivatives.[23] Not only does this method enable location of half power points, but it is also an

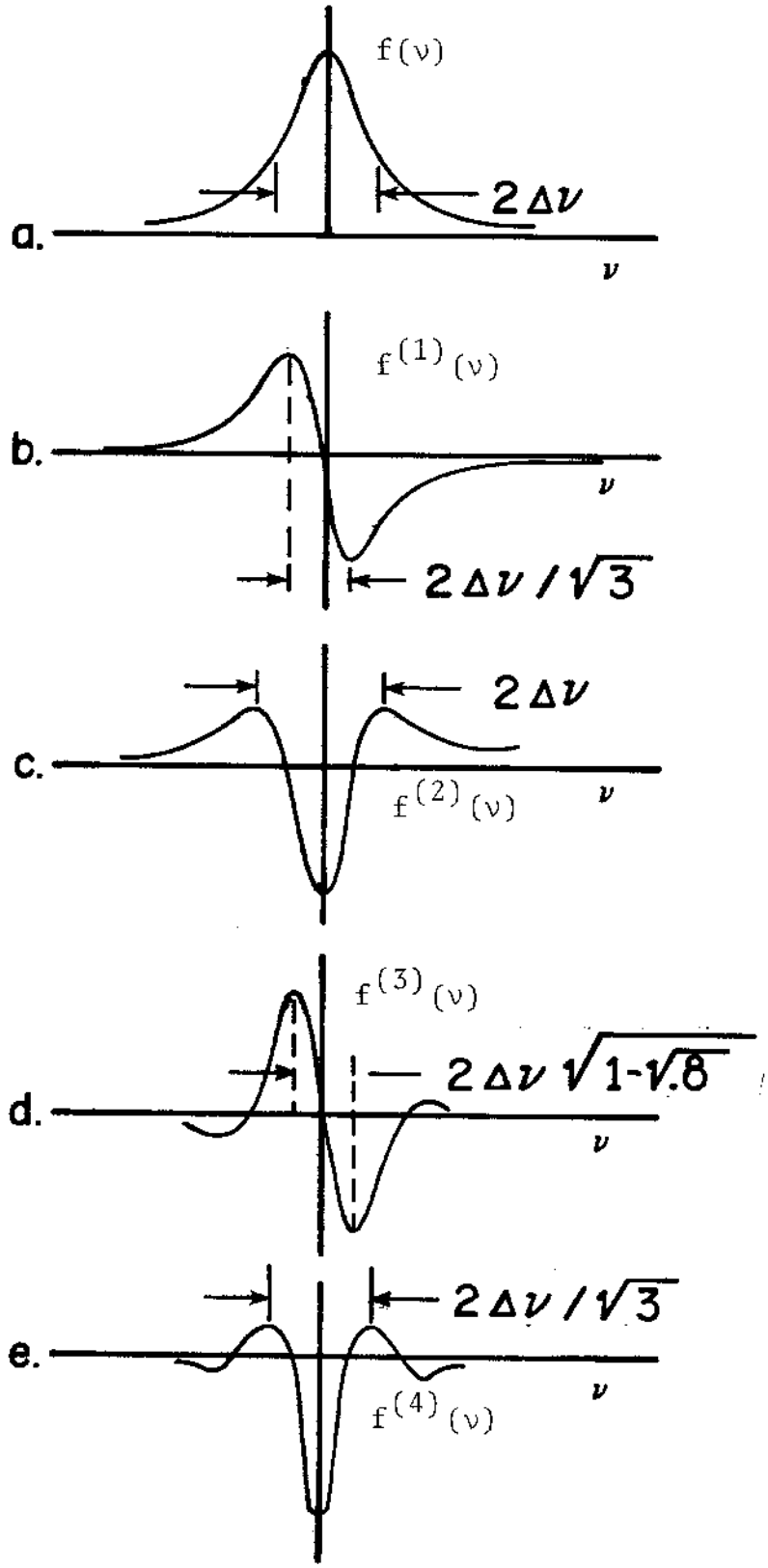


Figure 3. The Lorentzian line shape $f(\nu)$ and its derivatives $f^{(n)}(\nu)$, where(a). $f(\nu)$,(b). n=1, (c). n=2, (d). n=3, (e). n=4.

excellent method of determining the shape of a resonance profile. It is apparent that determining the position of a peak is far more precise than finding the half-power points of an absorption line, particularly considering that a variable background may shift the peak height significantly, but alters its position almost negligibly. It has been shown also that differentiation greatly improves the resolution of a spectrograph.[24]

However, the modulation process also changes the frequency incident upon the molecules, which results in further broadening of the absorption line. Rinehart[22] has applied the theory of Karplus[21] to the case of low amplitude and slow modulation. Quantitatively, his results are valid for cases in which both the peak frequency excursion of $\Delta f$ and the rate of modulation $f_1$ are numerically less than the half-width of the line under investigation, i.e.,

$$\Delta f < \Delta\nu \qquad\qquad f_1 < \Delta\nu \ .$$

The measured half width, $\delta\nu$, of the first derivative of an absorption line modulated by a sine wave is related to the pressure-broadened width by[22]

$$\delta\nu = \frac{\Delta\nu}{\sqrt{3}}\left\{1 + \frac{1}{2}\left(\frac{f_1}{\Delta\nu}\right)^2 + \frac{3}{4}\left(\frac{\Delta f}{\Delta\nu}\right)^2\right\} \tag{7}$$

where $\delta\nu$ is the observed half width, $\Delta\nu$ is the true half

width, $\Delta f$ is the modulation amplitude, and $f_1$ is the modulation frequency. This allows the parameter of interest, $\Delta\nu$ to be extracted from the experimentally measured value $\delta\nu$.

For the case of modulation whose amplitude is larger than allowed by the approximations mentioned above, a more general approach has been developed by Netterfield _et al._[23] A power coefficient $\alpha$ is calculated from the instantaneous rate of energy absorption from the modulated microwave field at time $t_o$, bearing in mind that this rate of absorption depends on the modulation as well as the energy stored previous to $t_o$. A synopsis of this development follows.

Referring to Appendix B for a development of the expression of the net energy stored, $W(t_o)$, we write

$$W(t_o) = \int_0^\infty a_m^*(t_o)a_m(t_o)\ (h\omega_{mn})^2\ \frac{f_n N}{kT\tau}\ \exp(-\theta/\tau)d\theta \quad (8)$$

where $a_m(t_o)$ is the probability amplitude for a transition, $h\omega_{mn}$ is the energy difference between the two states, $(N/\tau)\exp(-\theta/\tau)d\theta$ describes the number of particles undisturbed by collisions for a period of time $d\theta$ in a system where $\tau$ is the mean time between collisions, $f_n$ is the fraction of total molecules in state n, k is Boltzmann's

constant, and T is the absolute temperature. Now if we define $\beta(t)$ to be the rate of absorption of energy from the microwave field, we can rewrite $W(t_0)$ as[23]

$$W(t_0) = \frac{1}{\tau}\int_{\theta=0}^{\infty}\int_{t_0-\theta}^{t_0} \exp(-\theta/\tau)\beta(t)dtd\theta. \tag{9}$$

If the frequency of modulation is $\omega_1$, $\beta(t)$ can be expressed as a Fourier sum of the fundamental frequency and its harmonics,[23]

$$\beta(t) = \sum_{k=-\infty}^{\infty} C_k \exp(ik\omega_1 t). \tag{10}$$

Making the substitution of Eq. (10) for $\beta(t)$ into Eq. (9) and integrating yields,[23]

$$W(t_0) = \tau\sum_{k=-\infty}^{\infty}\frac{C_k}{1+ik\omega_1\tau}\exp(ik\omega_1 t_0) = \sum_{k=-\infty}^{\infty} W_k \exp(ik\omega_1 t_0) \tag{11}$$

where $C_k = W_k(1+ik\omega_1\tau)/\tau$. $W_k$ corresponds to the energy extracted from the $k^{th}$ harmonic of the modulation frequency.

To determine the absorption coefficient $\alpha$, consider that P, the average value of the Poynting vector, is[23]

$$P = \frac{1}{2}\left[\frac{\varepsilon_0}{\mu_0}\right]^{\frac{1}{2}} E_0^{\,2}. \tag{12}$$

The absorption must be equal to the attenuation of P. Therefore,[23]

$$\frac{\partial P}{\partial z} = -\beta(t) = -2\left[\frac{\mu_0}{\varepsilon_0}\right]^{\frac{1}{2}} \frac{\beta(t)}{E_0^{\,2}} P = -\alpha P \tag{13}$$

so that $P = P_o \exp(-\alpha z)$ where[23]

$$\alpha = 2\left[\frac{\mu_o}{\varepsilon_o}\right]^{\frac{1}{2}} \frac{\beta(t)}{E_o^{\,2}} . \tag{14}$$

For propagation through a layer of gas,[23]

$$P = P_o \exp(-\alpha \ell) \simeq P_o(1-\alpha\ell) . \qquad (\alpha << \ell) \tag{15}$$

Using equations (10) and (14), we have for the emf generated[23]

$$\varepsilon = \gamma P = \gamma P_o - 2\gamma P_o \left[\frac{\mu_o}{\varepsilon_o}\right]^{\frac{1}{2}} \frac{1}{E_o^{\,2}} \sum_{k=-\infty}^{\infty} C_k \exp(ik\omega_1 t) . \tag{16}$$

Since $W(t_o)$ is real,[23]

$$C_k = C_{-k}^{*} = E_o^2 (p_k + iq_k)^{\frac{1}{2}} \tag{17}$$

and it follows that[23]

$$\frac{1}{E_o^{\,2}} \sum_{k=-\infty}^{\infty} C_k \exp(ik\omega_1 t) = P_o + 2 \sum_{k=1}^{\infty} \left\{ p_k \cos(k\omega_1 t) + q_k \sin(k\omega_1 t) \right\} \tag{18}$$

and so $\varepsilon_k$, the coefficient of the $k^{th}$ harmonic of $\varepsilon$ is[23]

$$\varepsilon_k = 4\gamma P_o \ell \left[\frac{\mu_o}{\varepsilon_o}\right]^{1/2} (p_k^2 + q_k^2)^{1/2} . \tag{19}$$

For sinusoidal modulation, the electric component of the microwave field is[23]

$$E = E_o \cos(\Phi(t)), \tag{20}$$

such that $d\Phi/dt = \omega_0 - \omega \sin\omega_1 t$ where $\Delta\omega/2\pi = \Delta f$ is the modulation amplitude, $\omega_0/2\pi = \nu_0$ is the center frequency of the radiation, $\omega_1/2\pi = f_1$ is the frequency of modulation. Substituting the expression for $\Phi(t)$ into Eq. (20) yields[23]

$$E(t) = E_0 \cos\left(2\pi\nu_0 t + \frac{\Delta f}{f_1}\cos(2\pi f_1 t)\right), \tag{21}$$

which can be rewritten in terms of Bessel functions of the first kind as[25]

$$E(t) = E_0 \sum_{n=-\infty}^{\infty} J_n\left[\frac{\Delta f}{f_1}\right] \cos\left\{2\pi(\nu_0 + nf_1)t + \frac{n\pi}{2}\right\}. \tag{22}$$

Subsequent tedious manipulation yields expressions for $p_k$ and $q_k$ that define the coefficient of the emf corresponding to the $k^{th}$ harmonic,[23]

$$\left.\begin{array}{l}\text{for even } k,\ (-1)^{k/2} p_k \\ \text{for odd } k,\ (-1)^{(k-1)/2} q_k\end{array}\right\} = D \sum_{n=-\infty}^{\infty} J_n\left[\frac{\Delta f}{f_1}\right] J_{n+k}\left[\frac{\Delta f}{f_1}\right]$$

$$\times \left[\frac{2\Delta\nu \quad + \frac{1}{\Delta\nu}((\nu'+nf_1)^2 + (\nu'+(n+k)f_1)^2)}{8\pi^3(\Delta\nu^2+(\nu'+nf_1)^2)(\Delta\nu^2+(\nu'+(n+k)f_1)^2)}\right] \tag{23}$$

$$\left.\begin{array}{l}\text{for odd } k,\ (-1)^{(k+1)/2} p_k \\ \text{for even } k,\ (-1)^{k/2} q_k\end{array}\right\} = D \sum_{n=-\infty}^{\infty} J_n\left[\frac{\Delta f}{f_1}\right] J_{n+k}\left[\frac{\Delta f}{f_1}\right]$$

$$\times \left[\frac{((\nu'+nf_1)(\nu'+(n+k)f_1)/\Delta\nu^2 - 1)kf_1}{2\pi(\Delta\nu^2+(\nu'+nf_1)^2)(\Delta\nu^2+\nu'+(n+k)f_1)^2)}\right] \tag{24}$$

$$\text{for } k = 0,\ p_0 = 2D \sum_{n=-\infty}^{\infty} J_n^{\,2}\left[\frac{\Delta f}{f_1}\right]\left[\Delta\nu(2\pi^3)((\nu' + nf_1)^2 + \Delta\nu^2\right]^{-1} \quad (25)$$

where

$$D = \omega_{mn}^{2} f_n N |\mu_{x_{mn}}|^2 / 4kT\tau^2. \quad (26)$$

$\mu_{x_{mn}}$ is the dipole moment matrix element connecting the two states and N is the total number of molecules in the system. So we have[23]

$$\varepsilon_k = B(p_k^{\,2} + q_k^{\,2})^{\frac{1}{2}} \quad (27)$$

where

$$B = 4\gamma P_0 \left[\frac{\mu_0}{\varepsilon_0}\right]^{\frac{1}{2}}. \quad (28)$$

With this result we have an expression for an absorption line profile when the probing radiation is modulated sinusoidally. Since a sinusoidal modulation is used, this profile must be employed. Not only must the modulation shape be considered for the absorption line, but Doppler contribution must be considered.

## Doppler Broadening

If the molecular motion parallel (and anti-parallel) to the direction of propagation of the microwave radiation is considered, it is apparent that the frequency of absorption (or emission) that is observed will be Doppler shifted from the value that would be expected if the molecules were at rest with respect to the radiation field. If the

z-component of molecular velocity is small compared to c, the speed of light, then the Doppler shifted frequency is[23]

$$\nu'' = \nu(1 \pm v_z/c). \tag{29}$$

The fraction of molecules having a velocity between $v_z$ and $v_z + \delta v_z$ is governed by the Maxwellian velocity distribution, and is given by[23]

$$\frac{\delta N_{v_z}}{N} = \left[\frac{m}{2\pi kT}\right]^{1/2} \exp\left[\frac{-mv_z^2}{2kT}\right]\delta v_z \ . \tag{30}$$

Considering the energy absorbed from the modulated wave as before and including the Doppler shift by replacing $\nu$ by $\nu''$ in Eqs. (23) and (24), the contribution to the $k^{th}$ harmonic of the emf must be integrated over all possible velocity components parallel and anti-parallel to the direction of progagation $v_z$. This gives as the expression for the line shape corresponding to the $k^{th}$ derivative[23]

$$\mathcal{E}_k = B(P_k^2 + Q_k^2)^{1/2} \tag{31}$$

where

$$\left.\begin{array}{l} \text{for even k, } (-1)^{k/2} P_k \\ \\ \text{for odd k, } (-1)^{(k-1)/2} Q_k \end{array}\right\} = D\sum_{n=-\infty}^{\infty} J_n\left(\frac{\Delta f}{f_1}\right) J_{n+k}\left(\frac{\Delta f}{f_1}\right) \tag{32}$$

$$\times \int_{-\infty}^{\infty} \frac{\left\{2\Delta\nu + (\nu' + nf_1 + \frac{\nu}{c}v_z)^2 + (\nu' + (n+f)f_1 + \frac{\nu}{c}v_z)^2/\Delta\nu\right\} e^{-mv_z^2/2kT} dv_z}{2\pi^2(\Delta\nu^2 + (\nu' + nf_1 + \frac{\nu}{c}v_z)^2)(\Delta\nu^2 + (\nu' + (n+k)f_1 + \frac{\nu}{c}v_z)^2)}$$

$$\left.\begin{array}{l}\text{for odd } k,\ (-1)^{(k+1)/2} p_k \\ \text{for even } k,\ (-1)^{k/2}\ Q_k\end{array}\right\} = D\sum_{n=-\infty}^{\infty} J_n\left(\frac{\Delta f}{f_1}\right) J_{n+k}\left(\frac{\Delta f}{f_1}\right)$$

$$\times\int_{-\frac{\nu}{c}}^{\infty} \frac{\left[(\nu'+nf_1+\frac{\nu}{c}v_z)(\nu'+(n+k)f_1+\frac{\nu}{c}v_z)/\Delta\nu^2-1\right] kf_1 e^{-mv_z^2/2kT} dv_z}{2\pi^2(\Delta\nu^2+(\nu'+nf_1+\frac{\nu}{c}\ v_z)^2)(\Delta\nu^2+(\nu'+(n+k)f_1+\frac{\nu}{c}v_z)^2)}. \quad (33)$$

## Overlapping Lines

It has been shown that there is a strong nuclear quadrupole interaction with the molecular electron cloud which results in hyperfine splitting of the principal transition energy level[27]. In some cases, the degree of separation was easily resolved with the spectrograph used. However, pressure broadening resulted in a merging of the lines which were well resolved at low pressure into a single line at higher pressures. The measured width of this composite line is related to the individual line widths in a manner which depends on the spacing of the component lines as well as their relative intensities. This effect is made clear in Figure 4 as the width of the resonance is advanced over a range of $\Delta\nu$ of twenty to two hundred kilohertz.

If the assumptions can be made that each component of the profile line has the same width at a given pressure and that each component has the same functional dependence which incorporates any of the broadening effects discussed above, then it can be further assumed that the entire

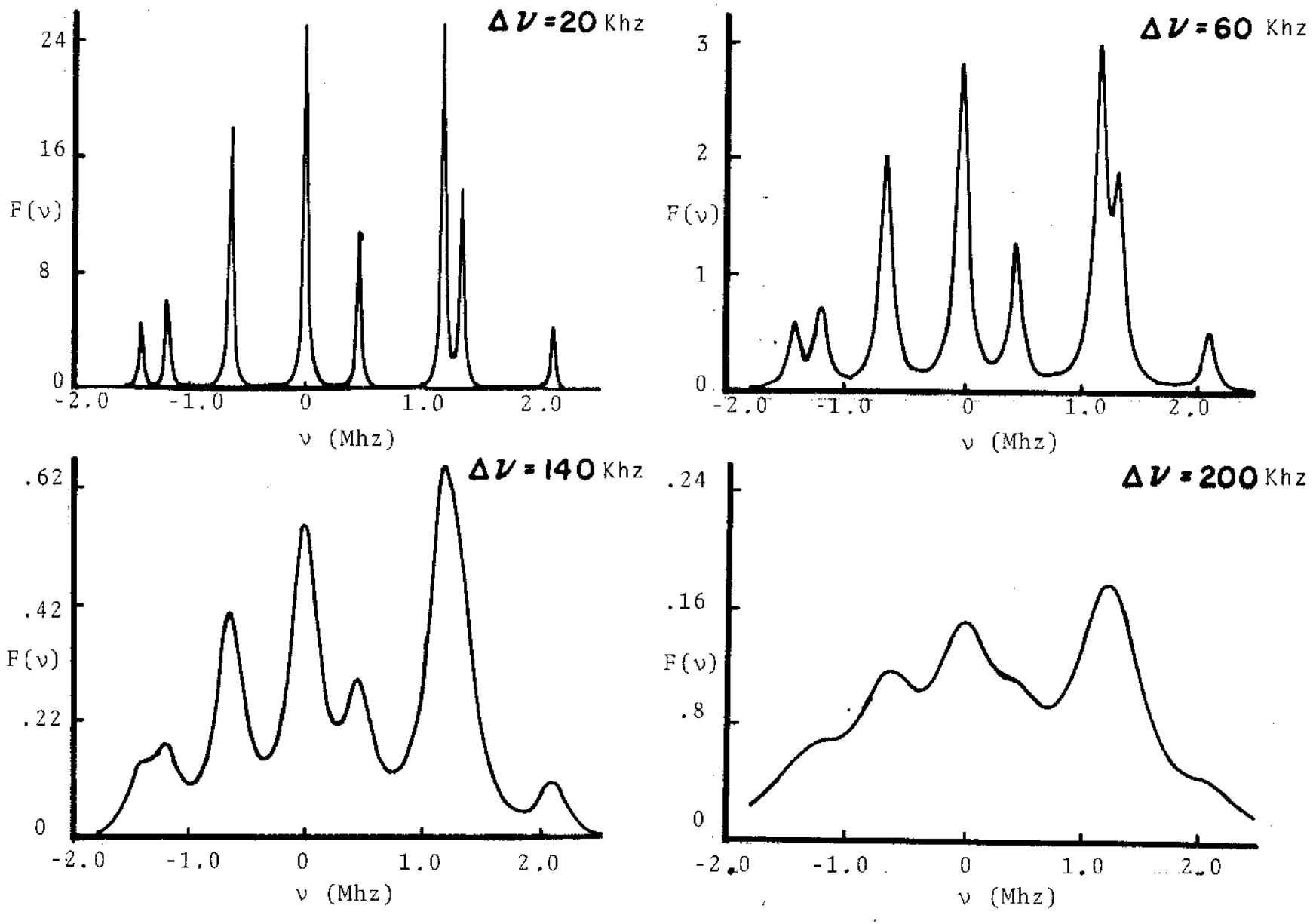


Figure 4. Model of a pressure broadened Lorentzian profile, scaled in arbitrary units. (J-J'=2-3)

absorption profile can be described by a linear sum of each component line, viz.,

$$F(\nu) = \sum_{i=1}^{N} f_i(\nu) \tag{34}$$

where N is the number of hyperfine components present in the transition under consideration.

In order to determine the origin and spacing of the hyperfine lines, Appendix A will be referred to as justification for a quadrupole interaction energy with an explicit form given in terms of molecular parameters and quantum numbers by Eq. (A-10). Incorporating as many effects as are detectable in the particular case of methyl cyanide, the total energy of a molecular state can be written as[26]

$$W_{tot}(J) = BJ(J+1)+(C-B)K^2-D_J J^2(J+1)^2 - D_{JK}K^2J(J+1)-D_K K^4+eqQ\left(\frac{3K^2}{J(J+1)}\right)f \tag{35}$$

where B is the rotational constant in megahertz, J is the total angular momentum, $D_{JK}$ is the coefficient of centrifugal distortion, eqQ is the quadrupole coupling strength, K is the projection of J along the molecular axis, and f is Casimir's function tabulated in reference 14. Only the energy difference between states is of interest, so we write

$$W = W_{tot}(J+1) - W_{tot}(J)$$

$$W = 2B(J+1) - 2D_{JK}K^2(J+1) - 4D_J(J+1)^3 \qquad (36)$$
$$+ eqQ\ 3K^2\{\frac{J(f'-f)-2f}{J(J+1)(J+2)} + f-f'\}$$

where f' is simply Casimir's function evaluated for J+1. Equation (36) was evaluated with the use of tables for the allowed transitions to obtain the frequency of each hyperfine line.[28] By the theorem of spectral stability, the intensities of the components of the spectral line must sum to the total expected intensity of the single composite line. In the situation being described here, this applies to the "family" of lines corresponding to a single K value. These relative intensities are also tabulated.[28] The relative intensities of the respective K values must also be known to scale properly the contribution of each hyperfine component. The relative intensities are given by[29]

$$I \propto |\mu_{ij}|^2 = \mu^2\{\frac{(J+1)^2 - K^2}{(J+1)(2J+1)}\}g(K) \qquad (37)$$

where g(K) = 2 for K = 1,2,3,... and g(K) = 0 for K = 0. Utilization of the vector coupling rules results in the energy level diagram illustrated for the J-J' = 1 - 2 transition in Figure 5. Figure 6 shows which transitions are allowed by selection rules, $\Delta J=1$, $\Delta K=0$, $\Delta F=-1,0,1$. It is these transitions which result in the complex spectra observed for methyl cyanide.

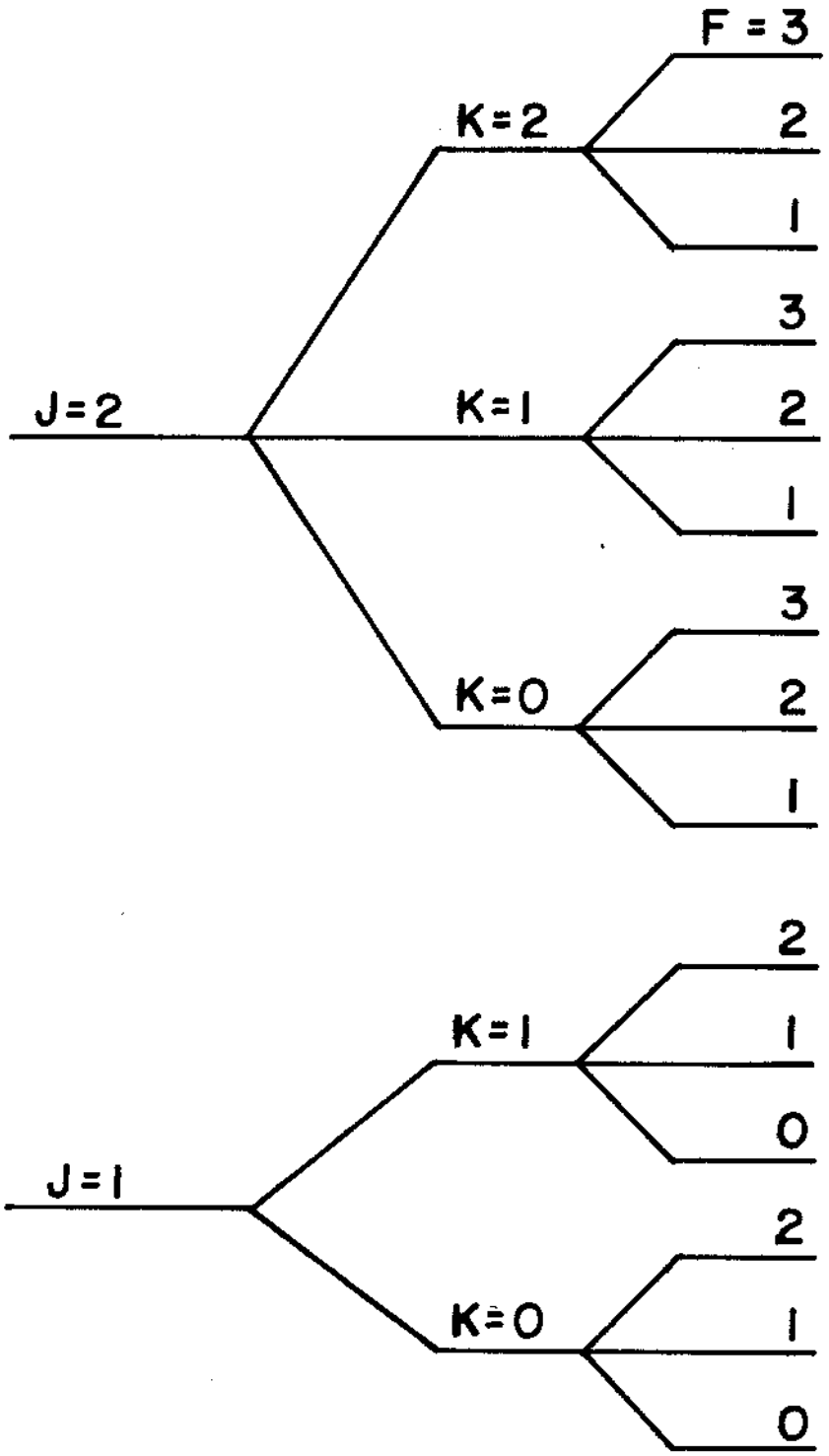


Fig. 5--Energy levels that result from vector coupling rules applied to $CH_3CN$.

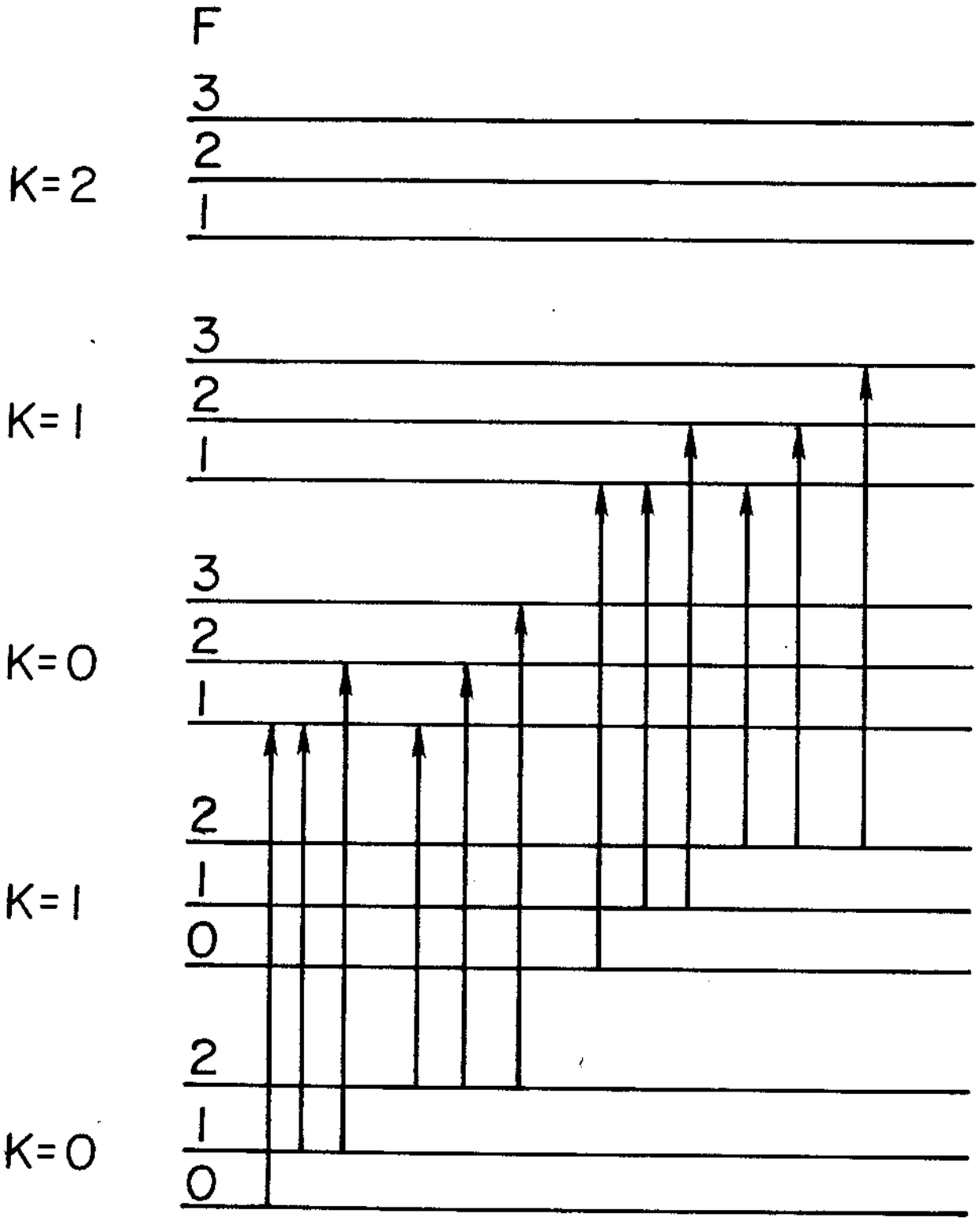


Fig. 6--Branches of the rotational energy levels $J$-$J'$= 1 - 2 of the $CH_3CN$ molecule. These levels are responsible for overlapping lines in the $J$-$J'$= 1 - 2 rotational level.

When a given line shape is assumed and the contribution from each hyperfine component is summed, as per Eq. 34, the resulting profile exhibits the distortion of line shape due to overlapping spectral lines. A family of the curves was generated by varying the half width $\Delta\nu$ to obtain a simulated pressure dependence for the complex spectra. Figure 7 shows this dependence for a Lorentzian line shape and for the Netterfield model of Eq. (32),[23] which incorporates modulation broadening and Doppler broadening to more closely simulate experimental results. When a comparison is made of $\Delta\nu$ for the Lorentzian line and the Netterfield model, the cumulative effect of the several broadening mechanisms can be compared. This provides then a method of deducing a true line width parameter when dealing with complex spectra.

This "true" line width parameter of interest is a measure of line broadening due to molecular collisions, which is pressure dependent.

The results obtained in this chapter are used in analyzing the experimental results of Chapter V. The following chapter outlines the major points of some of the current theories of spectral line shape.

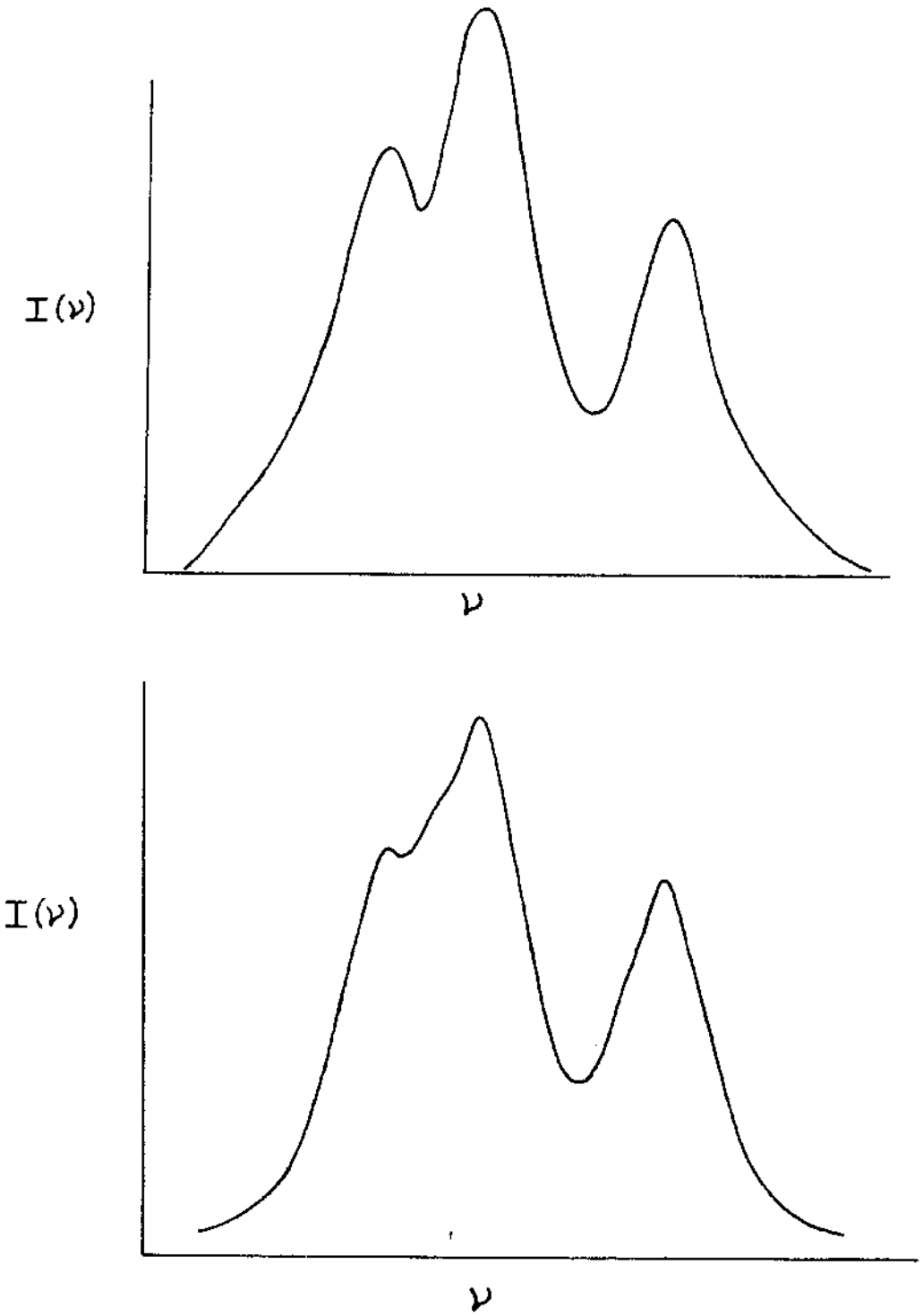


Fig. 7--Three major hyperfine components of the J-J' = 1-2 transition of $CH_3CN$. Above, Lorentzian line shape; below, Netterfield model.

# CHAPTER III

## THEORY OF PRESSURE BROADENING

A great deal of theoretical work has been done on the problem of pressure broadening of spectral lines, as this appears to be the dominant cause of line width. The significance indicated by this interest prompts a brief survey of the more successful theories. As might be imagined, the environment of a radiator largely determines the nature of any interactions which will affect the radiator, and hence its radiative output. Quantitative information about these interactions is what is sought from the investigation of spectral lines.

Theories of pressure broadening divide themselves into two distinct categories: (i) statistical theories and (ii) impact theories. The statistical theories of Kuhn and London[30] and Margenau[31] both examine the molecular environment with consideration of the spatial distribution of perturbers around an absorber. The potential due to this configuration determines how the absorber will either absorb or emit radiation. Obviously, this configuration must exist for a long time compared to the radiative process (or equivalently, the state lifetime) for any calculated effect to be meaningful. This restricts the validity of

the theory to slowly changing potentials, which, according to Margenau, may be realized at low temperature or high pressure. It has been found, however, that this statistical theory can provide a lower limit on the broadening characteristics of permanent dipoles (e.g., $NH_3$) or quadrupoles (e.g., oxygen). In view of these limitations, further discussion will pertain only to theories utilizing the impact approach.

## Impact Theories

Two basic assumptions are necessary for the application of impact theory. They are (i) the duration of the collision must be short compared to the mean time between collisions; that is, the term "moment of impact" is meaningful, and (ii) the molecules follow classical trajectories; that is, the wave packet describing the molecule must be well localized and its motion must be predicted by the laws of classical mechanics. For simplicity it will be assumed further that all collisions are binary. This condition is easily fulfilled at low pressures, ($P \leq 30$ mtorr), wherein this investigation was made. Various impact theories are now discussed.

### Van Vleck and Weisskopf

H. A. Lorentz[1] considered an oscillator forced by a periodic electric field and assumed that the oscillators

were randomly distributed after a collision. However, his result was not in agreement with that obtained by Debye[2] for the case of non-resonant absorption. Van Vleck and Weisskopf[5] modified this approach by stipulating that the molecules obey a Boltzmann distribution for a Hamiltonian function, which seems to be more physically applicable in the microwave region. The resulting line shape of Van Vleck and Weisskopf is given by[5]

$$f(\nu_{ij},\nu) = \frac{\nu}{\pi\nu_{ij}} \left\{ \frac{\Delta\nu}{(\nu_{ij}-\nu)^2+\Delta\nu^2} + \frac{\Delta\nu}{(\nu_{ij}+\nu)^2+\Delta\nu^2} \right\} \quad (38)$$

where $\nu_{ij}$ is the center frequency of the transition. This does indeed reduce to Debye's equation for non-resonant absorption and is still widely used for comparison of line shape parameters.

## Anderson

One of the most widely used of the modern collision theories is that due to P.W. Anderson.[6] Anderson used a Fourier integral approach which consists of a Hamiltonian which is the sum of an unperturbed Hamiltonian, $H_o$, and a time-dependent interaction Hamiltonian, $H_1$. Then following the lines of general radiation theory, Anderson derived the spectral intensity as a function of $\omega$, the angular frequency,

$$I(\omega) = C\omega^4 \mathrm{Tr}\ \rho_o \int_{-\infty}^{\infty} dt\ e^{i\omega t}\mu_z(t) \int_{\infty}^{\infty} dt' e^{-i\omega t'}\mu_z(t') \quad (39)$$

where $\rho_o$ is the initial density matrix of the gas and $\mu_z(t)$ is the time-dependent operator for the z-component of the dipole moment operator which satisfies the commutation relation

$$i\hbar\dot{\mu} = -(H\mu - \mu H), \tag{40}$$

The solution of this equation is

$$\mu(t) = T^{-1}(t)\exp(iH_o t/\hbar)\mu_o \exp(-iH_o t/\hbar)T(t) \tag{41}$$

where

$$i\hbar\dot{T}(t) = H_1'(t)T(t)$$

and

$$H_1'(t) = e^{iH_o t/\hbar} H_1(t) e^{-iH_o t/\hbar} . \tag{42}$$

The phase shifts due to the interaction $H_1'(t)$ are given by the diagonal elements of the matrix T(t). The absolute squared values of the off-diagonal elements are the transitional probabilities between states connected by this operator.

Anderson treated the standard optical case by assuming that if the collisions were short compared to the time between collisions, then the collisions were uncorrelated. In other words, the molecule has no memory of a past collision by the time another collision occurred. He showed that the collision cross-section $\sigma$ can be written as the sum of real and imaginary parts,

$$\sigma = \sigma_r + i\sigma_i \tag{43}$$

and derived an expression for the intensity distribution as[6]

$$I(\omega) = \frac{C(2nv\sigma_r)}{(\omega-\omega_{if}-nv\sigma_i)^2 + (nv\sigma_r)^2} \tag{44}$$

where $nv\sigma_r$ is $2\pi$ times the line half width $\Delta\nu$, and $nv\sigma_i$ is $2\pi$ times the frequency shift $\delta\nu$.

In order to facilitate computation of $\sigma$, Anderson defined an impact parameter b for a binary collision by[6]

$$r^2 = b^2 + v^2t^2 \tag{45}$$

for a binary collision, shown schematically in Figure 8. If b is averaged over all equivalent directions we have[6]

$$\sigma = \int_0^\infty 2\pi b S(b)\,db \tag{46}$$

where S(b) is a "collision efficiency" or weighting function which describes the effectiveness of a collision in perturbing the molecular state. Anderson showed that S(b) can be written as a sum of real and imaginary parts, $S_2(b)$ and $S_1(b)$ respectively,[6]

$$S(b) = S_1(b) + S_2(b) \tag{47}$$

where $S_1(b)$ is responsible for causing frequency shifts and $S_2(b)$ is responsible for causing pressure broadening of the spectral lines. Anderson assumed that for any event with $b \leq b_0$

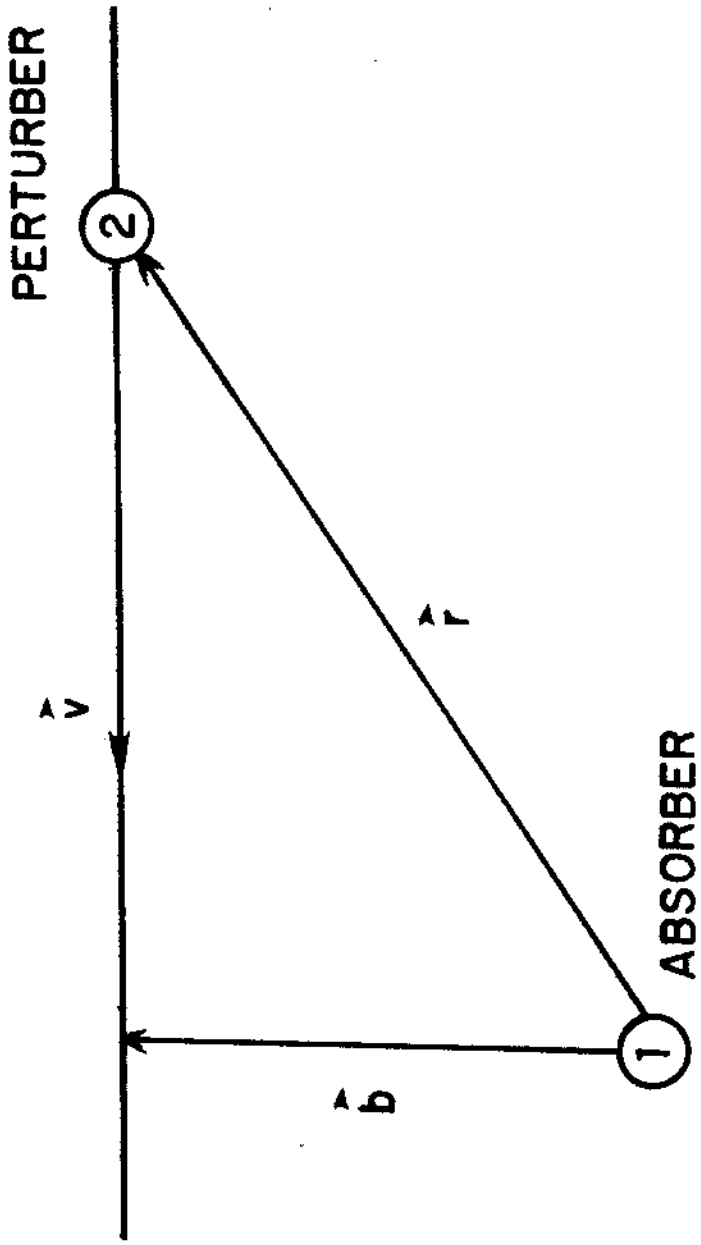


Fig. 8--Schematic of a collision between molecules (1) and (2) assuming a classical path for the interaction.

where $b_0$ is some assignable minimum impact parameter, then a collision and radiation interruption is assumed, that is,[6]

$$S_2(b_0) = 1 , \tag{48}$$

so that the collision cross section for broadening, $\sigma_r$, can be expressed[6]

$$\sigma_r = \pi b_0^2 + \int_{b_0}^{\infty} 2\pi b S_2(b) db. \tag{49}$$

Many expressions for $S_2(b)$ corresponding to various interaction types are available in the literature and so serve as comparison for experimental results for $\sigma$. For instance, Birnbaum[31] states a general form for $S_2(b)$ involving the states of the absorber and perturber as well as the type of interaction mechanism that predominates in collisions between various molecules. Tsao and Curnutte[8] have derived expressions for dipole-dipole, dipole-quadrupole, quadrupole-quadrupole, and dipole-induced dipole intermolecular potentials. Krisnaji and Srivastiva[32,33] have reported intermolecular potentials for first-order London dispersion and quadrupole-induced dipole forces.

## Murphy and Boggs

V. F. Weisskopf and E. Wigner[20] have shown that for $\overline{E}_i$ the average energy and $\tau_i$ the average lifetime of the $i^{th}$ state, the probability that the energy of this level

is in the range $E_i$ to $E_i + dE_i$ is[7]

$$W(E_i)dE_i = \frac{1}{\pi} \frac{h/4\pi\tau_i}{(E - \bar{E}_i) + (h/4\pi\tau_i)^2} dE_i. \tag{50}$$

Convolution of this yields the probability that the frequency of transition to state j, $\nu_{ij}$, is in the range $\nu_{ij}$ to $\nu_{ij} + d\nu_{ij}$,[7]

$$W(\nu_{ij}) = \frac{1}{\pi} \frac{1/\pi\tau_i + 1/\pi\tau_j}{(\nu_{ij} - \bar{\nu}_{ij})^2 + ((\frac{1}{4}\pi\tau_i) + (\frac{1}{4}\pi\tau_j))^2} \tag{51}$$

where $\bar{\nu}_{ij} = (\bar{E}_j - \bar{E}_i)/h$. Since the levels are being perturbed, $\bar{E}$ is not necessarily equal to $E^0$, the unperturbed energy. Therefore,[7]

$$\bar{\nu}_{ij} = \nu_{ij}^0 + \delta\nu_{ij} \tag{52}$$

where $\nu_{ij}^0$ is the unperturbed transition frequency and $\delta\nu_{ij}$ is the shift in center frequency due to collisions.

We now wish to find an absorption coefficient $\gamma$ which is the fractional intensity absorbed by a layer of gas of thickness $\ell$ per unit path length. For a dipole in a periodic electric field, the interaction Hamiltonian is[7]

$$H_{in} = -\vec{\mu}\cdot\vec{E}(t) = -\mu_z E(e^{2\pi i\nu t + i\alpha} + e^{-2\pi i\nu t - i\alpha}) \tag{53}$$

where z is along the electric vector, $\alpha$ is an arbitrary phase factor, and $\nu$ is the frequency of the electric field. Defining $\varepsilon = |E|/2$, it can be shown that the first-order

transition probability per unit time is[7]

$$W_{ij} = \frac{4\pi^2}{3h^3}\,\varepsilon^2|\mu_{ij}|^2\{\delta(\nu+\nu_{ij}) + \delta(\nu-\nu_{ij})\}. \tag{54}$$

The net energy absorbed from the field per unit volume per unit time is $(N_i-N_j)h\nu W_{ij}$. $N_i$ is the density of molecules in state i, and $\varepsilon^2 c/2\pi$ is the radiation flux. We have for the fraction of the intensity absorbed per unit path length,[7]

$$\delta\gamma_{ij}(\nu) = \frac{8\pi^3}{3ch}\,\nu(N_i-N_j)|\mu_{ij}|^2\{\delta(\nu+\nu_{ij}) + \delta(\nu-\nu_{ij})\}. \tag{55}$$

Using Eq. (51) to sum over $\nu_{ij}$, the average absorption coefficient is[7]

$$\gamma_{ij}(\nu) = \frac{8\pi^2}{3ch}\,\nu(N_i-N_j)|\mu_{ij}|^2\left\{\frac{\Delta\nu_{ij}}{(\nu-\nu_{ij}^0-\delta\nu_{ij})^2 + (\Delta\nu_{ij})^2} + \frac{\Delta\nu_{ij}}{(\nu+\nu_{ij}^0+\delta\nu_{ij})^2 + (\Delta\nu_{ij})^2}\right\}. \tag{56}$$

This defines the absorption line shape. The width is[7]

$$\Delta\nu_{ij} = 1/4\pi\tau_i + 1/4\pi\tau_j \tag{57}$$

and the shift is[7]

$$\delta\nu_{ij} = \frac{1}{h}\{(\bar{E}_j-E_j^0) - (\bar{E}_i-E_i^0)\}. \tag{58}$$

To examine the collision process, we consider a Hamiltonian

with an interaction potential. The Hamiltonian of an individual molecule is given by[7]

$$H = H^{o} + V(t), \tag{59}$$

where $H^{o}$ is the Hamiltonian of an isolated molecule and $V(t)$ is the time-dependent potential corresponding to a collision. To describe the collection of molecules, a time-dependent density matrix is formulated,[7]

$$\rho(t) = \exp(-i H^{o}t/\hbar)T(t)\rho(-\infty)T(t)^{-1}\exp(iH^{o}t/\hbar) \tag{60}$$

where[7]

$$i\hbar\frac{\partial T(t)}{\partial t} = \exp(i H^{o}t/\hbar)V(t)\exp(-i H^{o}t/\hbar)T(t). \tag{61}$$

The initial condition on the matrix $T(t)$ is that $T(-\infty) = \hat{I}$, the unit matrix. Further initial conditions are that $V(-\infty)$ be zero so that $\rho(-\infty) = \hat{1}$.

After the collision takes place, two situations are possible. The probability that the molecule is still in its initial level n, though perhaps phase-shifted, is[7]

$$\rho_{nn}(+\infty) = |T_{nn}(+\infty)|^{2}. \tag{62}$$

The probability that a transition has occurred is [7]

$$P_{n}(+\infty) = 1 - |T_{nn}(+\infty)|^{2}. \tag{63}$$

$T_n(t)$ can be evaluated from the following expression involving the collision potential[7]

$$\frac{\partial T_{ab}(t)}{\partial t} = -(i/\hbar)V_{aa}(t)T_{ab}(t) - (i/\hbar)\sum_{c\neq a} V_{ac}(t)\exp(i\omega_{ac}t)T_{cb}(t) \tag{64}$$

where $V_{ab}(t) = \langle a|V(t)|b\rangle$ is the matrix element connecting the two states a and b, and [7]

$$\nu_{ab} = (E_b^0 - E_a^0)/h. \tag{65}$$

$\nu_{ab}$ is the frequency corresponding to the energy difference of the unperturbed states a and b.

For "head-on" collisions, V(t) becomes very large so that the probability of a transition approaches unity. For simplicity, only direct transitions are considered, and the possibility of immediately relaxing back to a just vacated state is ignored. This tends to overestimate the transition probability, but good results are obtained for transitions involving widely spaced energy levels such as those characteristic of linear molecules and symmetric tops.

In order to compare directly the theory of Anderson[6] to that of Murphy and Boggs,[7] an expression for the "collision effectiveness" is desired. From Eq. (57), ignoring phase shifts, Murphy and Boggs obtained for the lifetime of state $J_1$[7]

$$\frac{1}{\tau_{J_1}} = \sum_{J_2} \rho_{J_2} \Phi(J_1 J_2) , \tag{66}$$

where $\rho_{J_2}$ is the density of states in the rotational level $J_2$. $\Phi(J_1 J_2)$ is the number of transitions per unit time from energy level $J_1$ due to collisions with molecules in level $J_2$ which can be written explicitly as[7]

$$\Phi(J_1 J_2) = 2\pi N \int_0^\infty b \, db \int_0^\infty vF(v)dv\{1-\exp -T_{J_1 J_2}(b,v) \}, \tag{67}$$

where N is the number of molecules per unit volume, F(v) is the Maxwell-Boltzmann velocity distribution, and b is the impact parameter. The term $T_{J_1 J_2}$ is evaluated by Murphy and Boggs from a perturbation expansion of the interaction matrix with a straight-line path approximation and is given by [7]

$$T_{J_1 J_2}(b,v) = 2S_2(b)_{0,i} . \tag{68}$$

$S_2(b)_{0,i}$ is Anderson's weight factor. Recall from Eq. (48) that Anderson assumed that any collision with impact parameter less than some minimum is "one hundred percent" effective. Murphy and Boggs explicitly averaged over velocity by evaluating the integrals in Eq. (67), which in general results in line width parameters that are

smaller than those of Anderson. The collision effectiveness functions are compared in Figure 9.

## Center Frequency Shifts

Both the theory of Anderson[6] and the theory of Murphy and Boggs[7] predict a shift due to collisions in the center frequency of an absorption line. It is further suggested that this shift is a function of the temperature of the absorbing gas.[23] The theory of Tsao and Curnutte[8] results in an expression for the absorption line shape that includes the center frequency shift as the parameter a multiplied by the half width of the line, where a has a value generally less than 0.1. According to the theory, then, the center frequency shift is a linear function of pressure, and is an extremely small effect. However, using the phase locking technique mentioned earlier, center frequency shifts have been observed for the self-broadened case of methyl cyanide, and the results of these observations are presented in Chapter V.

In the following chapter is a detailed description of the experimental instrumentation used in this investigation.

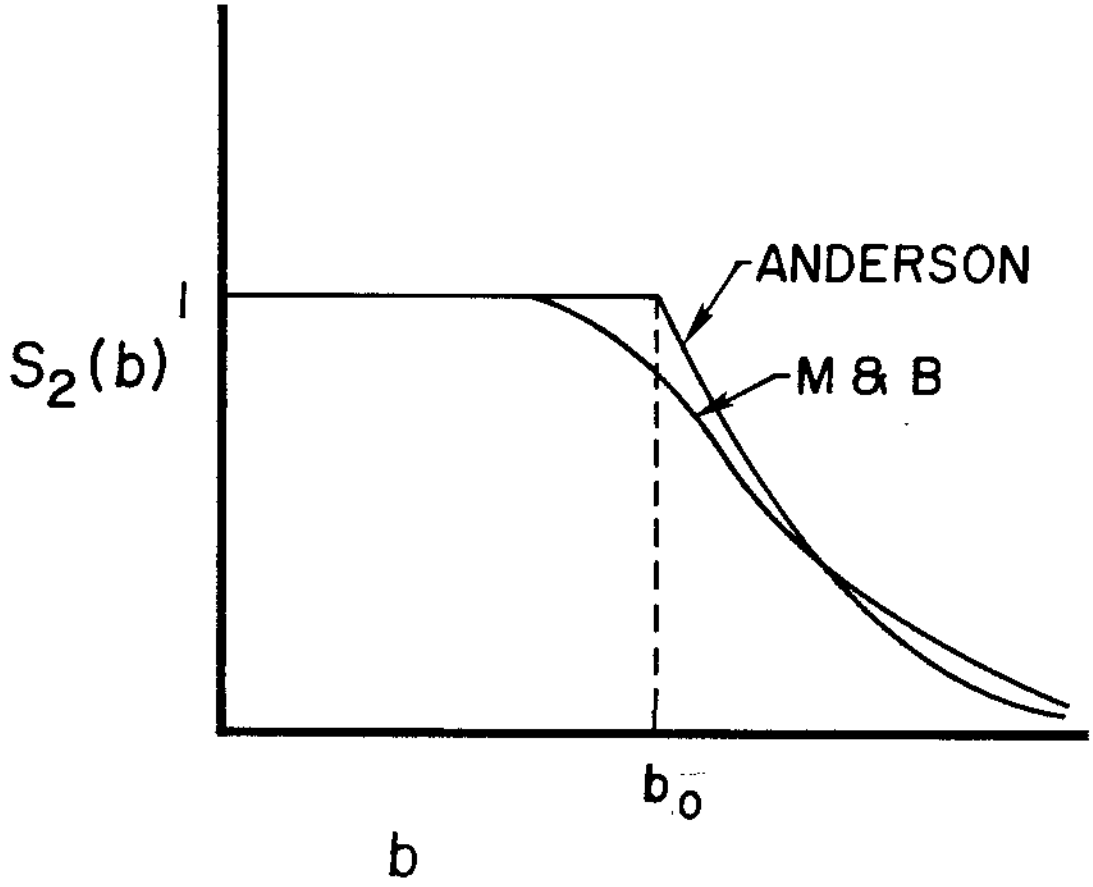


Fig. 9--Collision effectiveness function $S_2(b)$ as function of impact parameter b.

# CHAPTER IV

## INSTRUMENTATION

In order to observe molecular transitions in the microwave region and measure the parameters of interest that have been introduced, a spectrometer with good stability and a resolution on the order of a few tens of kilohertz is required. The specific equipment used to implement such a spectrograph will now be briefly described, having been reported extensively by Roberts.[18]

In a typical spectroscopic experiment, radiation is supplied from a source and guided through an absorption chamber to be detected and displayed in some fashion. One may then establish characteristics of the mechanical and electrical system, free of any complications from an absorbing material. The substance under investigation is then admitted into the absorption chamber in a gaseous form and the resulting absorption is detected and displayed. There must be some manner of calibrating the range of frequency employed in order to make quantitative measurements in the parameters of the absorption line. This typical procedure naturally divides itself into five areas of instrumentation and hardware as depicted in Fig. 10.

1. Radiation source and associated electronics;

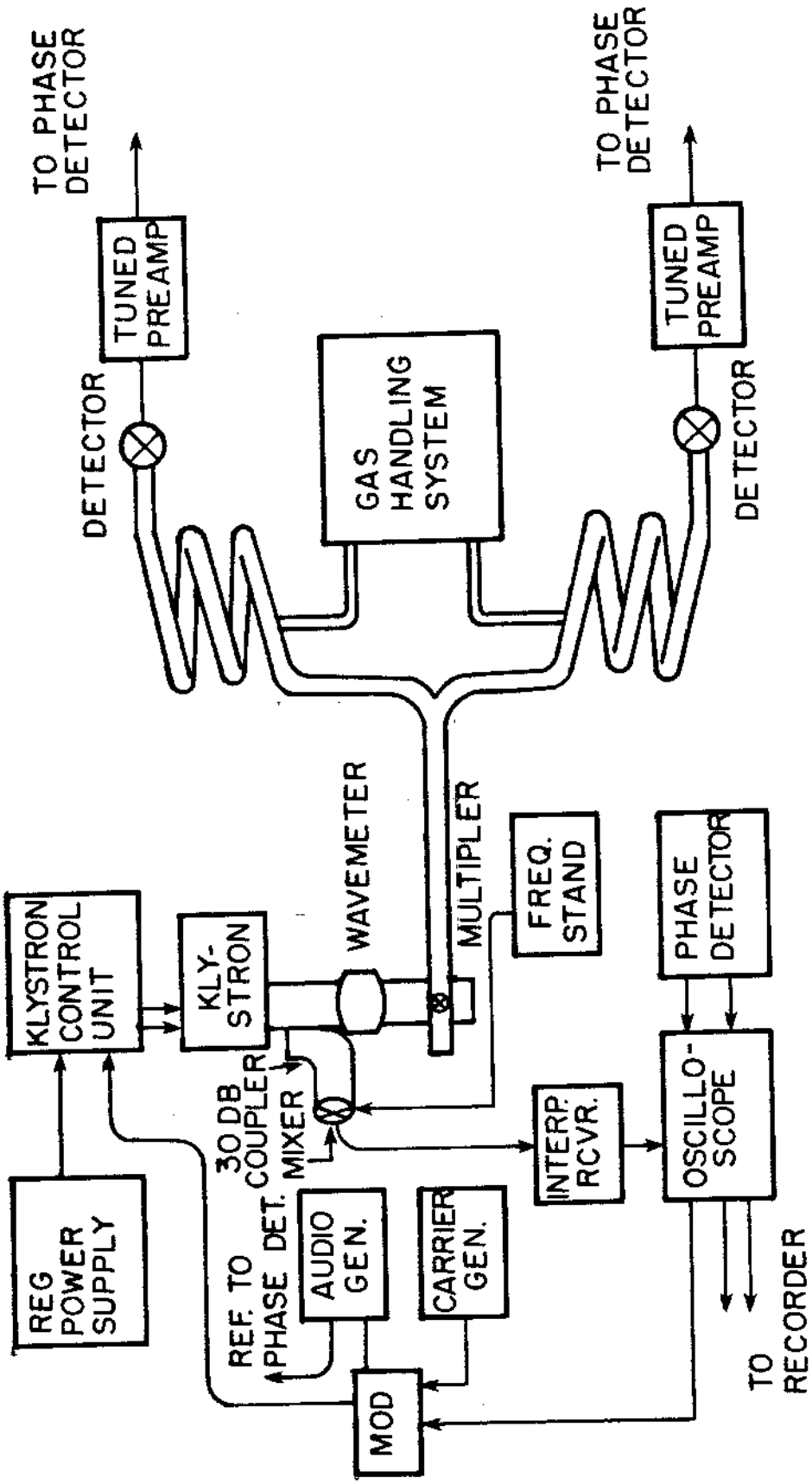


Fig. 10--Detailed schematic of spectrometer used in line width determination and line shift measurement.

2. absorption chamber;
3. detection and display;
4. gas handling system, and;
5. a frequency standard for calibration.

## Radiation Source and Controls

As mentioned earlier, reflex klystrons provide a stable, tunable source of virtually monochromatic microwave radiation. Klystron tubes manufactured by OKI and Varian were used, which produced frequencies in the range of the $CH_3CN$ transitions under investigation. For some transitions, the fundamental frequency of an available klystron was in the appropriate range; however, it was often necessary to double the fundamental using a diode multiplier. In one extreme case, two klystrons of different frequencies were summed together in the crystal multiplier to obtain the appropriate frequency. This method is not suggested, due to the multiplicity of harmonics, sums, and differences that are generated.

It is possible to sweep a range of frequencies by sweeping the repeller of the klystron with a voltage ramp available from the sweep of the oscilloscope. The frequency response of the klystron was measured by applying a control voltage to its repeller and indirectly measuring the frequency shift. As explained later, the klystron's

radiation was mixed with that of a precisely controlled oscillator to produce an intermediate frequency within range of an interpolation receiver. A typical value of klystron sensitivity indicates that a one-volt change in the repeller voltage will result in a one-megahertz change in the output frequency of the klystron. There are, of course, extreme cases to be found, and each klystron is highly individual in this respect. In all cases, a minimum range of ten megahertz was achieved with this technique. This range was measured by applying an offset voltage and directly observing the frequency shift of the klystron relative to the frequency markers.

To supply the high operating potential (up to 2.5 kilovolts) of the klystron, a Northeast-Scientific Corporation RE-1610 Regulated High-Voltage Supply was used with a Hamner N-4035 High Voltage Power Supply. This resulted in a well regulated voltage applied to the klystron anode and repeller. Since a one-millivolt ripple would result in a one kilohertz or larger frequency excursion of the klystron, tight regulation of the supply voltage is mandatory.

It has been mentioned that frequency modulation was employed to facilitate resolution, etc. This modulation voltage is also supplied to the repeller, having been supplied by a Heath EUW-27 Audio Frequency Generator. Isolation of this modulation voltage was achieved by a modulator

built in the electronics shop. This modulator impressed the low-voltage modulation onto the high-voltage supply and precluded the necessity of operating the modulation devices at a high potential. Voltage levels of three to four volts from the audio frequency generator were attenuated by the modulator to around three or four millivolts at the repeller of the klystron.

Coarse frequency adjustment of the klystron was achieved by mechanically altering the size of the klystron's resonant cavity by means of a flexible diaphragm and a cantilevered screw assembly. Fine frequency adjustment was available through fine adjustment of the repeller voltage.

## Absorption Cells

As indicated by Figure 10, there were two absorption cells used in this investigation, one for a standard pressure and temperature reference and one for observing dependence of the absorption parameters on these two variables. Both cells were equalized at the lowest pressure at which an absorption was measurable; then the reference cell was sealed and the absorption in it was used as an indicator of relative line broadening and absolute center frequency shift. A more precise measure of the line broadening was made using the frequency marker to be discussed later.

A thermal jacket was provided for the cell used for measurements so that it could be maintained at a desired

temperature for the duration of a set of measurements. Measurements were made at room temperature (297 K), ice water (273 K), and dry ice (194.5 K).

The ends of the cell were sealed with Teflon windows to allow changing transition sections and detectors without altering the pressure in the absorption cell. Teflon was selected over mica, for its ruggedness and availability, although the transmission characteristics may be slightly superior. Breaking the conduction path of the radiation in this manner gives rise to reflections which greatly enhance the standing wave pattern of the system. To combat this, the gaps were spaced to approximately $\lambda/4$ of the radiation used and transmission was significantly improved, much like the effect of a quarter wave plate in optics. This effect has been discussed in depth by Dagg et al.[35]

Two types of cells were used in this investigation, cylindrical copper tubing and rectangular aluminum waveguide. Townes and Schawlow[36] show an expression for optimum cell length to be $L = 2/a_o$, where $a_o$ is the attenuation constant, whose value is typically on the order of $10^{-3}$ $cm^{-1}$. A range of five to thirty meters results from this. Both types of cells were about twelve meters in length, thus satisfying the length criterion. Also of importance, both types of cells had cutoff frequencies well below any transition frequencies of interest. The inside diameter of

the cylindrical cell was two centimeters and the measurements of the rectangular cell were 1.8 centimeters by 2.5 centimeters. Both types were coiled with a mean diameter of about one meter, to facilitate storage.

After a series of measurements was made in the cylindrical cell, it appeared that the cell was suffering poor rectangular-to-cylindrical mode conversion with, consequent poor power transmission and generation of spurious modes whose absorption characteristics were unknown. Subsequent measurements were then made with the rectangular cell, and both sets of measurements are presented.

## Detection, Amplification, and Display

As mentioned previously, power levels incident on the detector were on the order of $10^{-8}$ watts, and resonant absorption by molecules may represent less than $10^{-6}$ of the ambient power level in the cell. It is these small absorptions that the detection system must follow in order to allow measurement of the absorption characteristics of a particular molecule. To achieve this degree of sensitivity requires precise matching of system components and extreme care in implementation.

Crystal diodes were used for primary detection: in the range from ten gigahertz to forty gigahertz, germanium 1N26 diodes were used, and above forty gigahertz, germanium

1N53 diodes were used. Voltage levels of five to twenty millivolts were amplified by a set of matched high gain bandpass pre-amplifiers constructed in the electronics shop. These amplifiers were tuned to thirty-two kilohertz to allow differentiation by modulation, as discussed earlier. From the pre-amplifiers, the signal was sent to two PAR-122 Lock-In Amplifiers used as phase-sensitive detectors, whose phase reference came from the Heath EUW-27 Audio Frequency Generator. A dual-trace Tektronix 502A oscilloscope provided visual display for the absorption, and a permanent record was made by a dual-pen Rika-Denki B201 Chart recorder. A typical recorder output is shown in Figure 11.

It should be pointed out that source modulation is to be desired, for several reasons. First, it greatly enhances the resolution of the spectrograph by displaying the rate of change of a quantity rather than the quantity itself (the quantity being the line shape, slope, inflection, etc., for increasing orders of derivatives). Modulation also allows the use of A-C amplification of the detected signal, which is far more effective than D-C amplification; noise is limited by bandwith, and crystal noise is reduced. It is possible to minimize linear and quadratic contributions to the standing wave background by observing the first and second order derivatives of the signal. Finally, it

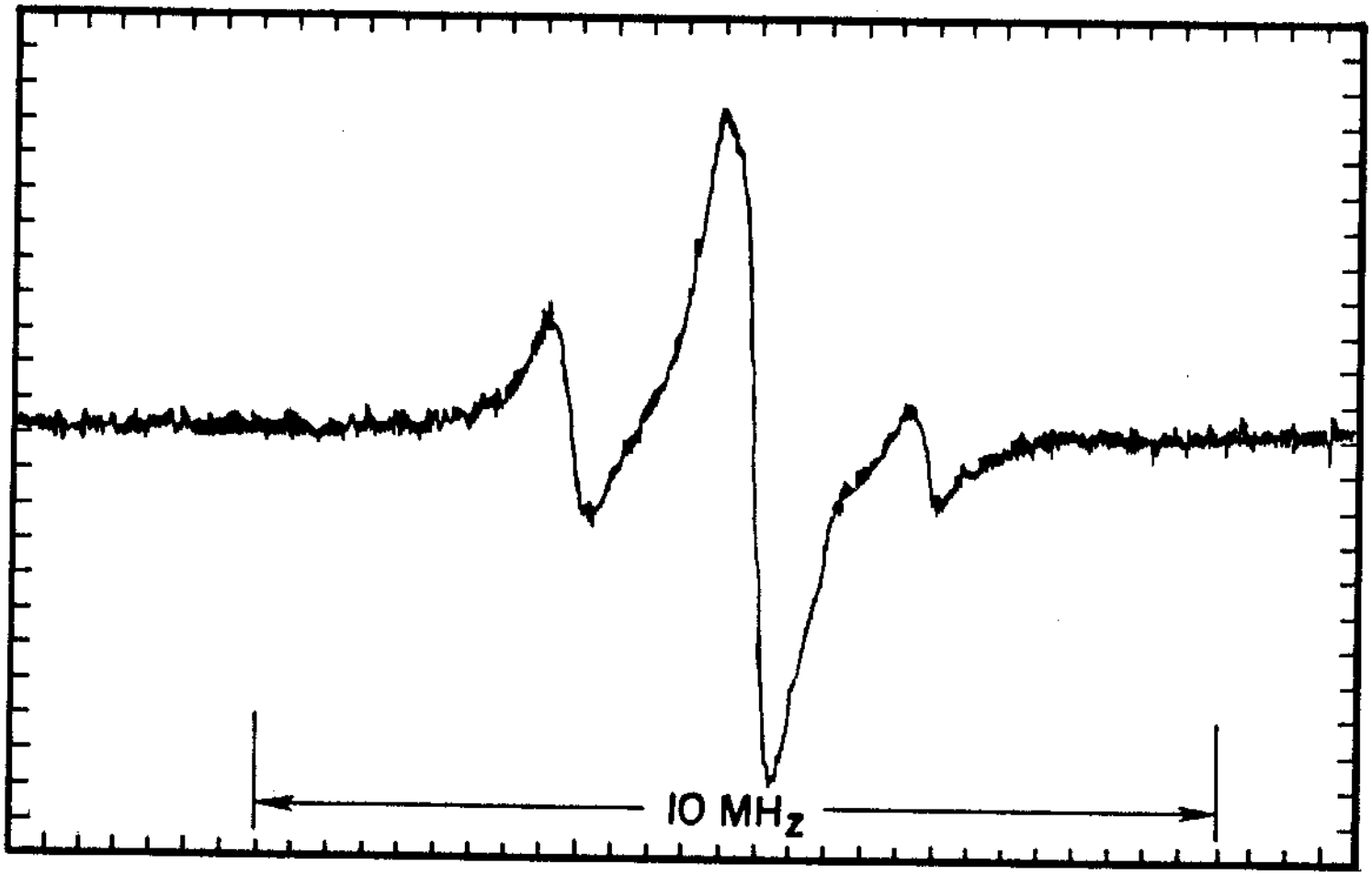


Fig. 11--Typical chart recorder tracing of a first derivative profile of the J-J' = 0-1 transition components in $CH_3CN$.

has been shown by Dagg et al.[35] that line shape distortion can be largely eliminated by observing higher order derivatives.

## Gas Handling System

Pressure in the absorption cell was controlled by a Van Waters and Rogers HV-1 oil vapor diffusion pump cold-trapped with liquid nitrogen. This was fore-pumped by a Welch Duo-Cell 1405 mechanical pump. The gas under investigation was admitted to the absorption cell from a liquid reservoir which had been pumped to remove residual air and water-vapor. The gas pressure in the absorption cell was measured by a Hastings Vacuum Gauge SV-1 which had been calibrated by a McLeod Gauge whose calibration is directly traceable to the the National Bureau of Standards. It was observed that $CH_3CN$ compresses readily, and only obeys the ideal gas law for low pressures. For this reason, the Hastings Gauge was calibrated using the lowest range of pressures which gave measurable differences in the mercury column heights in the McLeod Gauge. At these low pressures, the Hastings Gauge was found to have a linear correspondence to the McLeod Gauge, such that the direct reading multiplied by 0.41 gave the true gas pressure from the Hastings Gauge.

## Frequency Standard

In order to calibrate the range of the display for purposes of measurement, a well-known frequency interval must be recorded along with the absorption profile. A typical method of achieving this, and one which was used in this investigation, is to heterodyne the microwave frequency with a precisely known standard frequency and, receive the difference frequency which lies within the range of an available interpolation receiver. The receiver in this case was a Well-Gardner BC-348Q radio receiver, and a typical setting was 250 kilohertz, so that as the klystron frequency was swept through the range of interest, markers appeared at 250 kilohertz above and below the center line frequency, giving a total marker spread of 500 kilohertz.

The standard frequency was derived from a General Radio U2-B standard frequency multiplier slaved to a Hewlett-Packard quartz oscillator, resulting in a frequency stability of better than one part in $10^9$. Other more exotic frequency standards were employed, such as a phase-locked klystron slaved to a standard frequency. This provided a higher frequency for calibration, and the technique holds promise for locking the microwave source itself to give greater inherent stability to the spectograph.

# CHAPTER V

## ANALYSIS OF EXPERIMENTAL RESULTS

In this chapter, the experimental results of this investigation are presented and discussed. Line width measurements on transitions of the type $\Delta J = +1$ and $\Delta K = 0$ of the symmetric top molecule methyl cyanide are collected in Table II. Only self-broadening collisions are considered here at three different temperatures to investigate any temperature dependence of the line width parameter and line shift parameter.

All measurements reported here were made using the spectrometer described in detail in Chapter IV. Data analysis was performed to take into account all the relevant effects discussed in Chapter II. In particular, the Netterfield model[6] of modulation broadening and Doppler broadening was incorporated into a simulation of the absorption manifold by summing several individual lines, as discussed in Chapter II. The minimum amount of modulation required to clearly observe the second derivative profile was determined, and this modulation level, along with the absolute temperature, was used as a parameter in determining the amount of modulation and Doppler broadening,

TABLE II

EXPERIMENTAL VALUES FOR LINE WIDTH PARAMETERS

| Transition (JKF-J'K'F') | Temperature (K) | Frequency (MHz) | Line Width Parameter (MHz/Torr) | | | | Collision Diameter (Å) |
|---|---|---|---|---|---|---|---|
| | | | Experimental | | Theoretical | | |
| 001-102 | 300 | 18397.524 | 42.6±4.0 | | 91.67[b] | 77.0[d] | 21.8±1.0 |
| 102-203 | 300 | 36794.702 | 36.5±3.0 | 41.2[a] | 70.0[c] | 82.78[d] | 20.1±0.9 |
| 201-302, 212-313 | 300 | 55191.662 | 32.3±3.0 | | | | 18.9±0.9 |
| 203-304, 202-303 | 300 | 55191.937 | 30.8±1.4 | | | | 18.5±0.5 |
| 213-314, 211-312 | 300 | 55192.026 | 31.4±1.3 | | | | 18.7±0.4 |
| 102-203 | 273 | 36794.702 | 33.5±3.6 | | | | 18.8±1.0 |
| 101-202 | 273 | 36794.608 | 40.8±2.7 | | | | 20.8±0.7 |
| 203-304, 202-303 | 273 | 55191.662 | 36.9±1.7 | | | | 19.8±0.5 |
| 203-304, 202-303 | 195 | 55191.937 | 32.2±1.0 | | | | 17.0±0.3 |
| 201-302, 212-313 | 195 | 55192.026 | 30.0±1.2 | | | | 16.4±0.4 |

[a]Story, ref. 24.

[b]Anderson, ref. 6.

[c]Murphy and Boggs, ref. 7.

[d]Srivastiva, ref. 37.

using the equation developed by Netterfield et al.[6] This equation was evaluated and the results were plotted using a program encoded for and run on an IBM 360/50 computer and Cal-Comp Plotter software package. The superposition of several appropriately spaced lines was employed as a means to investigate the interaction of overlapping components within an envelope. The detailed analysis of profiles generated using this method resulted in the correction curves shown in Figures 12, 13, and 14 for each of the three transitions under consideration. For a given input of $\Delta\nu$, the pressure halfwidth, into the computer program listed in Appendix C, a half width $\delta\nu$ was measured from the resulting plot of the simulated absorption profile. This measured $\delta\nu$ represents the experimentally measured half width, which is a composite of all the broadening mechanisms. It was reasoned that the input $\Delta\nu$ should then be the pressure half width for the corresponding measured half width. The irregularity of the curves is almost totally attributable to the overlap of the hyperfine components, as evidenced by the J-J'=0-1 transition of Figure 12, which has widely spaced hyperfine structure, and the J-J'=1-2 and J-J/=2-3 transitions of Figures 13 and 14 respectively, which have closely spaced hyperfine lines. As can be seen from the correction

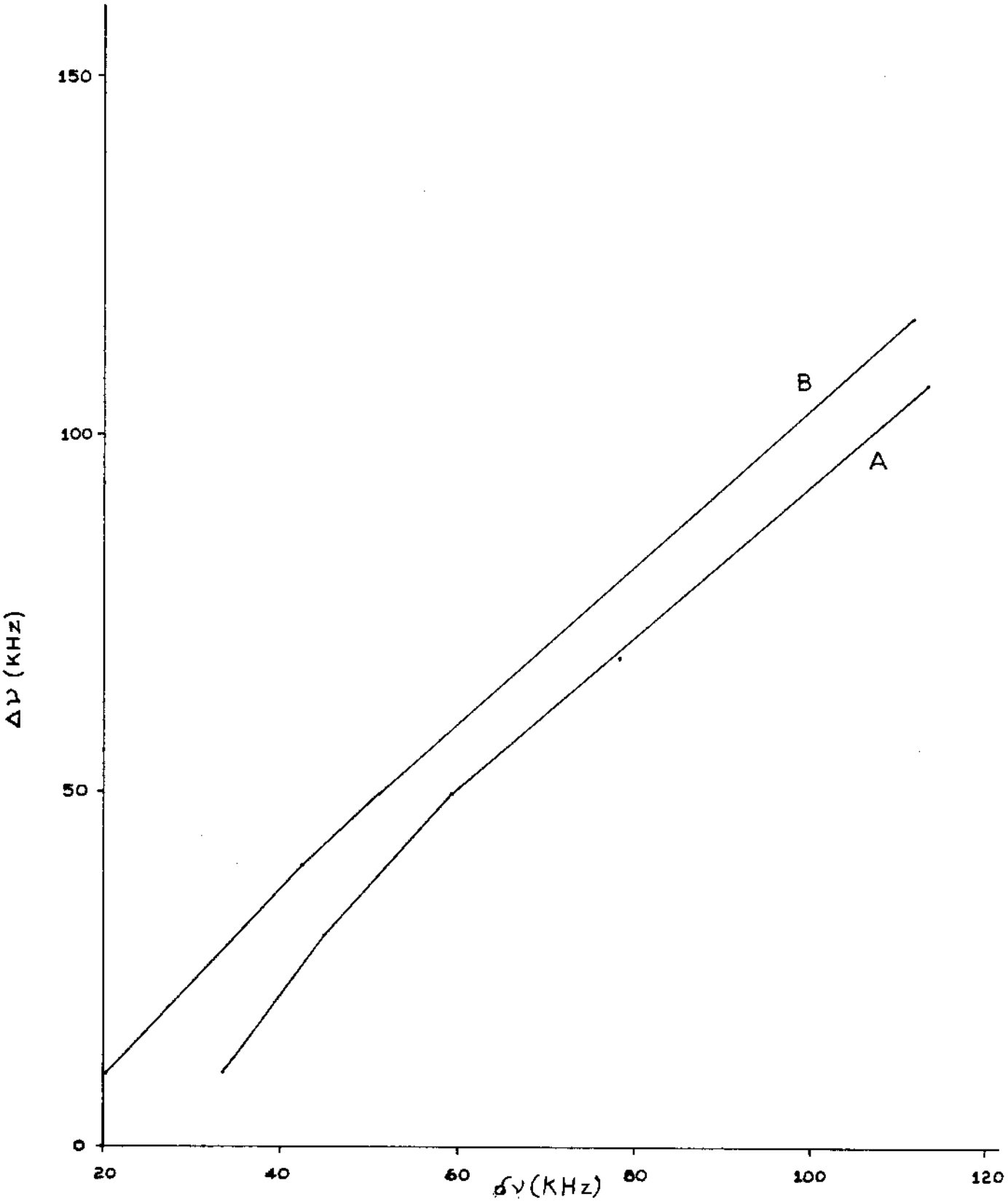


Fig. 12--Correction curves for the J-J' = 0-1 transition with a modulation width of 5 KHz. A is for the second derivative and B is for the fourth derivative.

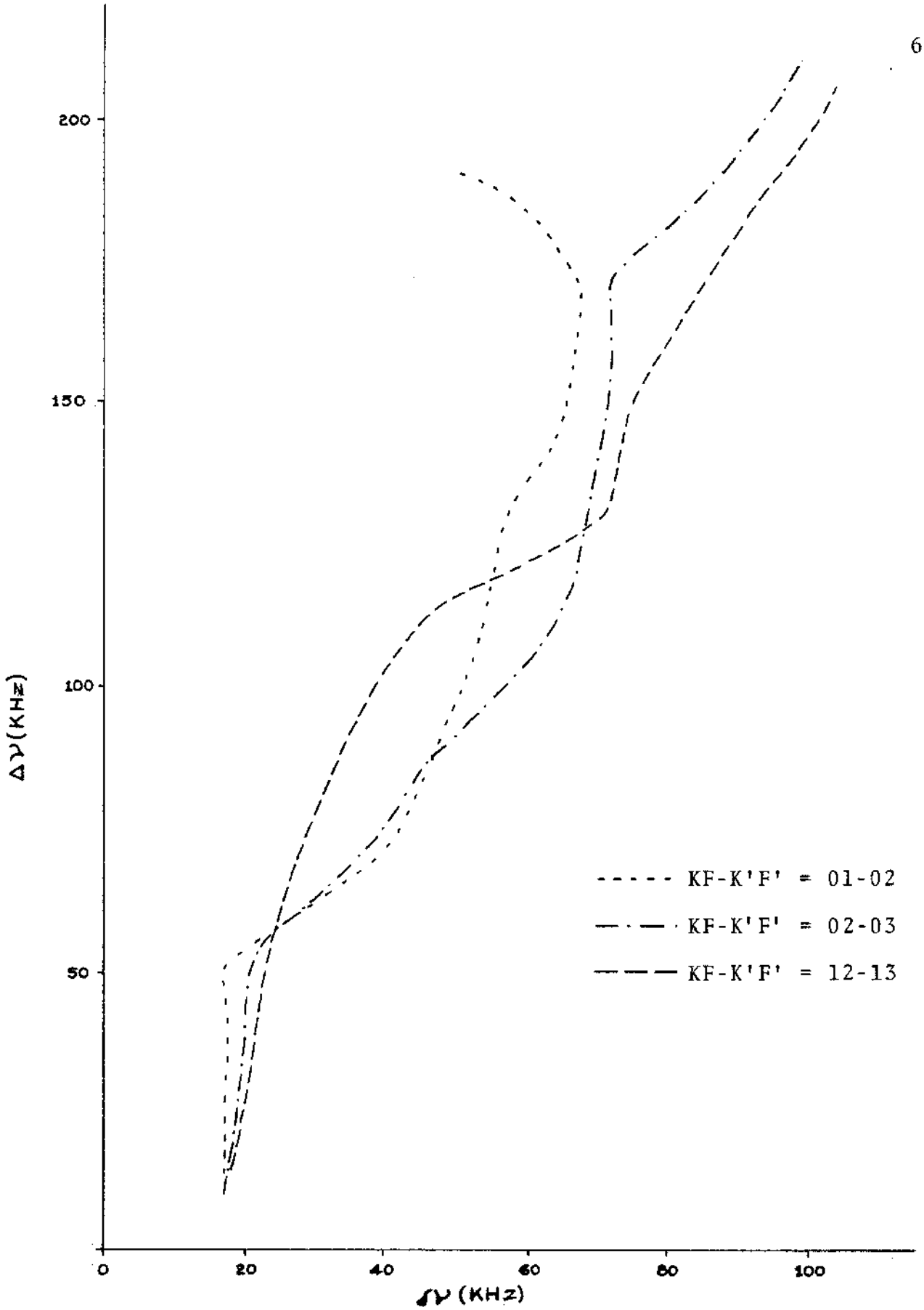


Fig. 13--Correction curves for the J-J' = 1-2 transition with a modulation width of 5 KHz, for the second derivative line shape.

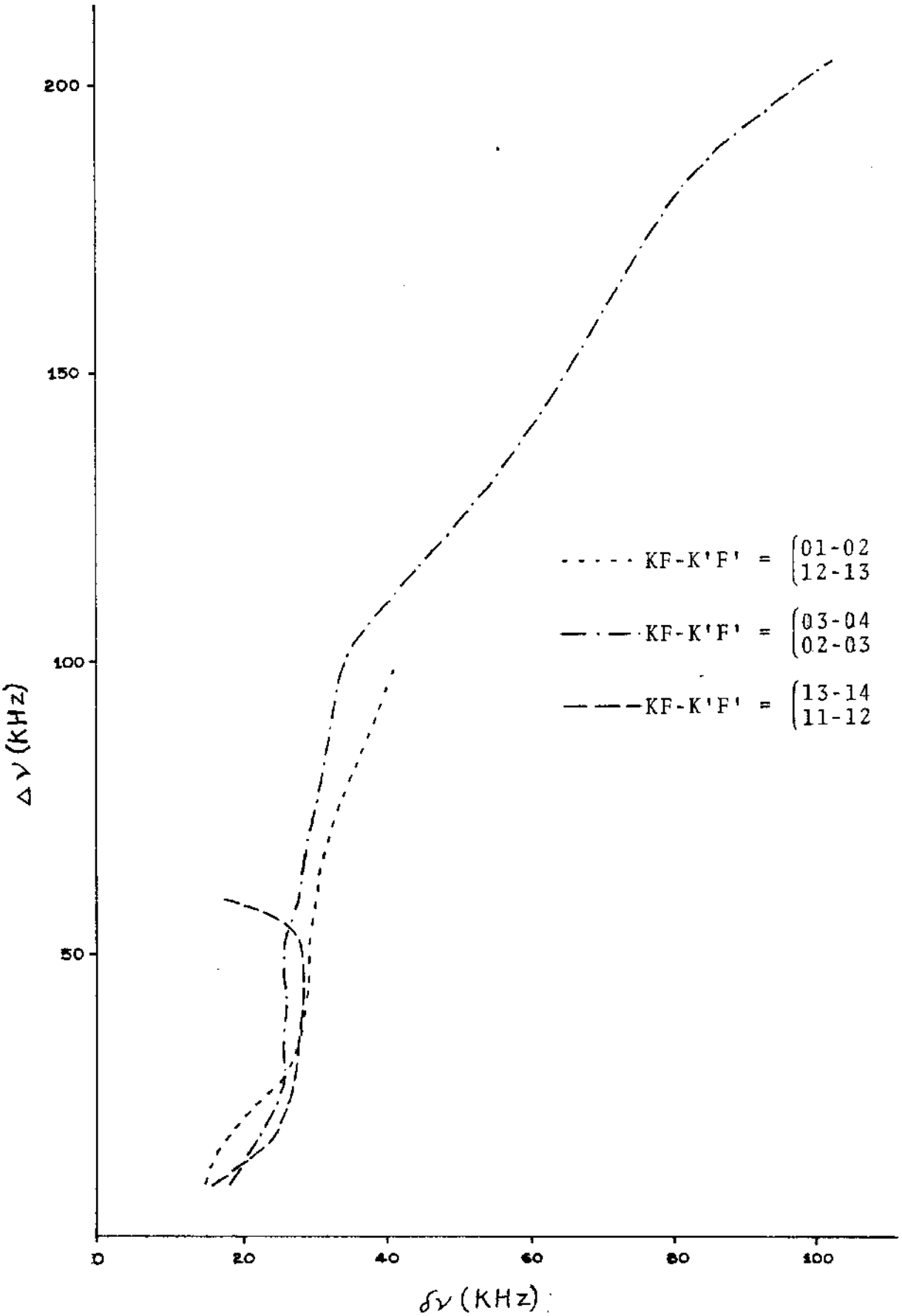


Fig. 14--Correction curves for the J-J' = 2-3 transition with a modulation width of 5 KHz, for the second derivative line shape

curves for the transitions which exhibit considerable overlap, the correction is a function of absolute line width, which introduces difficulties in that constant effects in the line width as well as relative changes must be determined. However, when these constant effects were minimized, this method of correction yielded satisfactory values for the line width parameters. For instance, the absorption cell described in Chapter IV and used in this work contributed a wall broadening at room temperature given by Gordy [4] as

$$\Delta\nu = \frac{1}{3\pi}\left|\frac{a+b}{ab}\right|\left[\frac{2kT}{M}\right]^{1/2} = 3.53 \text{ KHz} \tag{69}$$

where a and b are the rectangular dimensions of the cell. This width has a small but noticeable effect on the correction. With proper precautions, this method of analysis offers some insight into the complexities of overlapping spectra, an area which has been largely ignored experimentally because of the difficulties involved.

## Line Width Parameters

A typical plot of absorption line half width versus pressure is shown in Figure 15 to illustrate the extent of distortion produced by the overlapping spectra. Each point represents the average of at least five independent measurements. The "true" half width corresponding to each observed

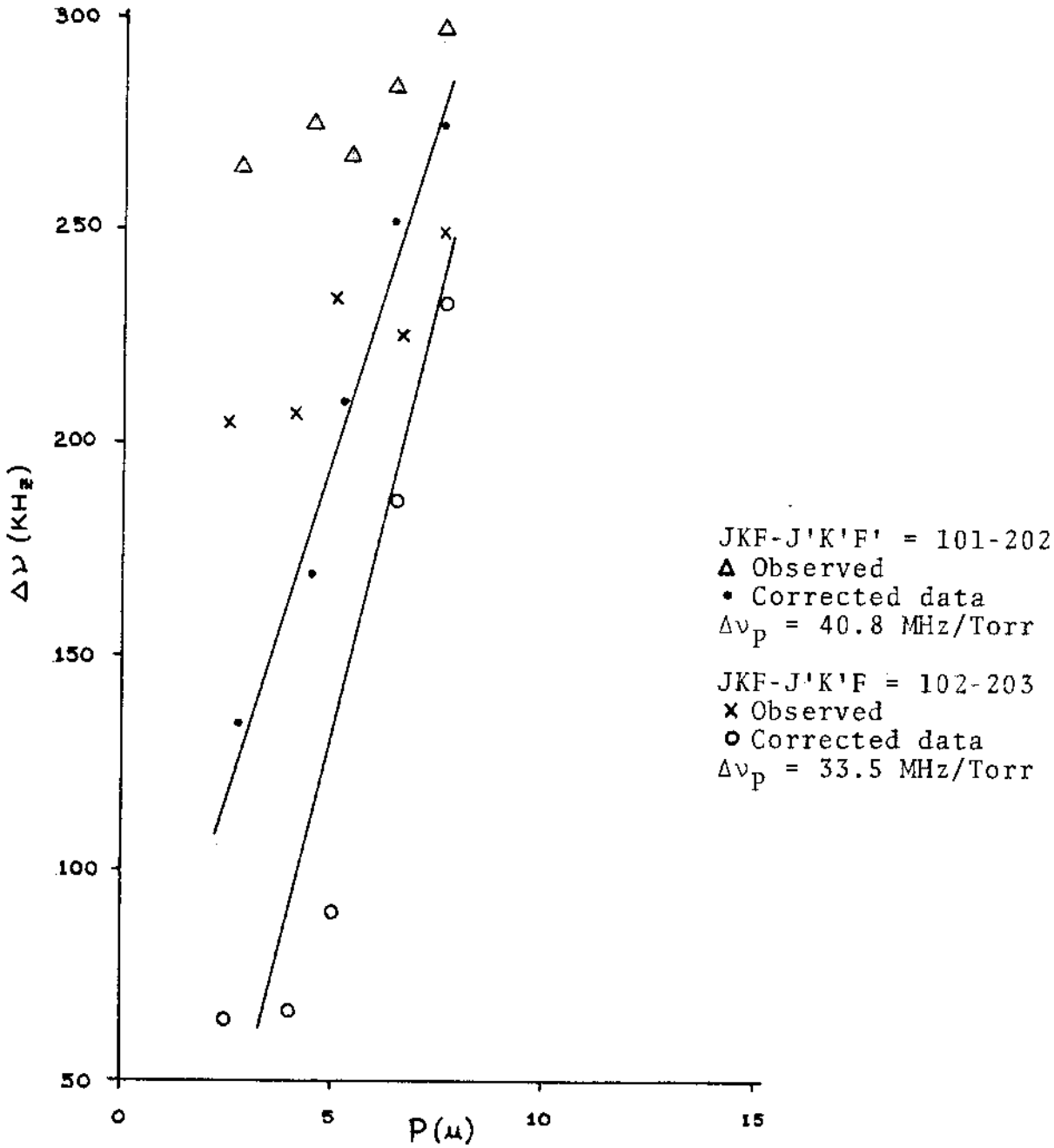


Fig. 15--Experimental data for the line width dependence on pressure for $CH_3CN$ at T = 273K for the J-J' = 1 - 2 transition.

half width was then determined from the appropriate correction curve and plotted against pressure. The line width parameter is the slope of this line, found from a linear least-squares fit of the data. The scatter in the data about the best straight line fit indicates not only the validity of the data but, in the case of severe overlap distortion, also the validity of the correction technique.

It is apparent from Figure 15 that the experimentally observed raw data may appear to deviate from the expected linear dependence on pressure in Eq. (5)

$$\Delta\nu = \frac{1}{2\pi\tau} = \frac{\eta\bar{v}\sigma}{2\pi}$$

When the correction for overlap is applied, it is seen that the data points are well described by a linear pressure dependence. While the correction is mathematically straightforward, the nature of the overlap distortion is such that a small error in measurement can result in a very significant error in the amount of correction applied to the data. Extracting the pressure half width from the measured half width consisted of matching the experimentally measured half width to a value of calculated half width on the correction curve and reading off the corresponding value of $\Delta\nu$, the pressure half width. Where the plot of $\Delta\nu$ versus $\delta\nu$ was not a single valued function, it was

assumed that an increase in pressure resulted in an increase in $\Delta\nu$, and ambiguities were thus avoided. Further refinement of this correction method should enhance the reproducibility of the results.

The theory of Anderson[6] predicts a decrease of $\Delta\nu_p$ with increasing energy, since collisions are not as effective in perturbing these higher-energy transitions. This trend is illustrated by the experimental results in Table II, but the values are not in agreement with the theoretical results in terms of relative magnitude. It is surprising to note that in the case of methyl cyanide, the calculated values of the line width parameter are significantly larg er than the experimental values. In all other cases of record, the theory predicts values smaller than those obtained experimentally. This is to be expected since the theory ordinarily accounts only for first-order effects in a particular molecular system, while the experiment reflects higher order interaction forces as well. The theory as applied to methyl cyanide apparently is not satisfactory.

The comparison of hyperfine components within the envelope of a transition is also of interest. It was demonstrated by Roberts _et al._[38] that the hyperfine components of $CH_3CL$ had the same value of $\Delta\nu_p$, within experimental error. In Table III, the available data

for $\Delta\nu_p$ show that the individual components of each transition do in general exhibit the same line width parameter. This was also indicated by preliminary results for the $J - J' = 0 - 1$ transition, the components of which were well resolved in the pressure range of this investigation. The lack of overlap removes the most obvious explanation of any dissimilarity in the individual $\Delta\nu_p$; that is, the distortion of the lines. A more fundamental question is raised about the effect of close-lying states on the transition probabilities of the levels under investigation. One method of removing this near degeneracy is to employ a Stark field to separate the individual components and study them as well-resolved lines. However, this precludes any interaction between adjacent levels by the removal of the near degeneracy. An investigation of this sort is suggested for future study and appears to hold promise of more insight into the problem of overlapping spectral lines.

The collision diameters listed in Table II are for self-broadening collisions, that is, $CH_3CN$ - $CH_3CN$ interactions, and the equivalent hardsphere diameters calculated are from Jeans,[39] using

$$b = (\Delta\nu_p)^{1/2} \, (M\pi kT/4N_o)^{1/4} \tag{70}$$

where M is the molecular mass, $N_o$ is Avogadro's number, and k is Boltzmann's constant.

## Error Estimate

Based on the reproducibility of the line width parameters, it is estimated that the listed values of $\Delta\nu_p$ represent a mean square error of less than 10. per cent. Aside from the uncertainty due to overlap, error also arises from three other major sources. First, standing waves introduce a shift and distortion that can be reduced but not eliminated by derivative techniques. Second, the method of measuring pressure is unsatisfactory. Slight nonlinearities are inherent in the Hastings gauge, and it has been found that the McLeod gauge used for calibration is reliable only for ideal gas approximations. This is the case at very low pressures for $CH_3CN$, so extrapolation to higher pressure was necessary with the Hastings gauge. A more satisfactory method of pressure measurement is currently under development. Third, the klystron sweep was slightly irregular, due to line voltage fluctuations, temperature variations, and vibration. As discussed in Chapter IV, this problem can be alleviated with the use of a phase-lock loop technique which promises good stability.

## Line Shift Measurements

According to the line shape derived by Tsao and Curnutte[8] from Anderson's impact theory[6], the shift in center frequency of the absorption line may be written as

$$\delta\nu_s = a\Delta\nu, \tag{71}$$

where $\Delta\nu$ is the half width at half maximum power and a is the line shift parameter. Anderson's theory states that a depends on matrix elements that are negligible for most types of interactions, which indicates that a will be quite small in general. Further, line shifts arise from adiabatic collisions which shift the phase of the molecular wave functions, but are of insufficient energy to stimulate transitions between energy levels. These collisions are believed to comprise a small fraction of molecular encounters, since the mean kinetic energy of the molecules at room temperature is much greater than the separation between energy levels. Considering this, it is expected that line shifts may become more prominent at reduced temperatures. For this reason, investigation was made into the behavior of the line shift parameter at various temperatures.

The line shift parameters collected in Table III were determined from measurement of the absolute shift in center frequency of the absorption lines under investigation. The absorption cell used as a reference was maintained at room temperature with a gas pressure just sufficient to observe the absorption. In this manner, both temperature dependence and pressure dependence were investigated simultaneously.

At low pressures, the envelope of the absorption was resolved into its component hyperfine lines; therefore it

TABLE III

EXPERIMENTAL DATA FOR LINE SHIFT PARAMETERS

| Transition (JKF-J'K'F') | Temperature (K) | Frequency (MHz) | Line Shift Parameter (MHz/Torr) |
|---|---|---|---|
| 001-102 | 300 | 18397.524 | 6.23 |
| | 273 | | - 2.33 |
| | 195 | | 1.20 |
| 001-101 | 300 | 18396.204 | 4.61 |
| | 273 | | 4.65 |
| | 195 | | .80 |
| 101-202 | 300 | 36794.608 | - .683 |
| | 273 | | -15.57 |
| | 195 | | - .833 |
| 102-203 | 300 | 36794.702 | - 4.62 |
| | 273 | | - 8.85 |
| | 195 | | - .689 |
| 112-213 | 300 | 36794.875 | -10.90 |
| | 273 | | -22.40 |
| | 195 | | - 4.95 |
| 201-302, 212-313 | 300 | 55191.662 | 7.45 |
| | 273 | | 1.57 |
| | 195 | | .227 |
| 203-304, 202-303 | 300 | 55191.937 | 5.06 |
| | 273 | | 2.16 |
| | 195 | | - .687 |
| 213-314, 211-312 | 300 | 55192.026 | - 1.098 |
| | 273 | | - |
| | 195 | | - .626 |

was on these components that the measurements were made. Experimental error arose from the unpredictable shift in center frequency, due to interaction of the overlapping lines within the envelope, as well as from shifts due to standing waves that would be present even in well-separated lines.

## Overlap-Induced Shift

The interaction of the individual hyperfine components results in a shift in the center frequency of each component that is sufficient to mask any expected collision-induced shift. However, the model of the absorption manifold can be employed to generate the expected overlap shift, so this effect can be removed from the data. This approach has been used by Story *et al.*[24] for the J-J' = 1-2 transition, with the result that the measured shift tracked the expected shift within limits of experimental error, indicating an absence of collision-induced shift.

An analysis involving all hyperfine components has been applied to all three transitions in this investigation. There is very little overlap shift evident in the J-J' = 0-1 transition in the pressure range under consideration, but the J-J' = 1-2 and J-J' = 2-3 transitions exhibit quite involved interaction, requiring application of an overlap correction. The shift parameters in Table III incorporate this correction where it is applicable.

## Standing Wave Shift

Standing waves result from reflections that are characteristic of cell geometry, and hence the standing wave pattern changes when changes in pressure or temperature alter the geometry of the cell even slightly. If the absorption line of interest is superimposed upon a standing wave, changes in the standing wave will result in shifts in the position of the center of the absorption line as well as distortions in the line width. Complete characterization of the standing wave may allow analysis of this standing wave shift, but such analysis was not included in this investigation.

In spite of the problems encountered in the measurement of center frequency shifts, the data was found to be generally a linear function of pressure, as expected. The spread in the data points is believed to be attributable to standing wave distortions.

## Comparison to Theory

While the behavior of individual components was regular, variations within the envelope were observed that apparently arise from small differences in the energy of the hyperfine transitions. The theory that predicts and describes the center frequency shift, notably that of Frost,[9] is not sufficiently developed to yield a detailed description of the experimental results for $CH_3CN$.

In determining a temperature dependence for the line shift parameter, it was found for the most part that the individual component parameters followed the same trend as the average. These trends are shown in Figure 16. A purely empirical description of the line shift parameter was presented by Frost[9] in an attempt to formalize this aspect of the line shift problem. It was suggested that a least-squares fit be made to the equation

$$y = C(1 + A \ln T)/ T^{x} \tag{72}$$

where C, A, and x are parameters. However, the experimental data in this investigation could not be satisfactorily fitted to this equation. A more complex theoretical problem underlies the subject of line shifts for $CH_3CN$. It has been suggested that any description should at least require information about the energy levels involved, and Eq. (72) does not explicitly contain an energy dependence upon the shift.

In conclusion, the investigation of the rotational transitions of $CH_3CN$ has resulted in precise measurements of the line width parameters of some low-lying transitions, and measurements of the shift in center frequencies of these transitions. The experimental results bear out the theoretical predictions where a comparison can be made,

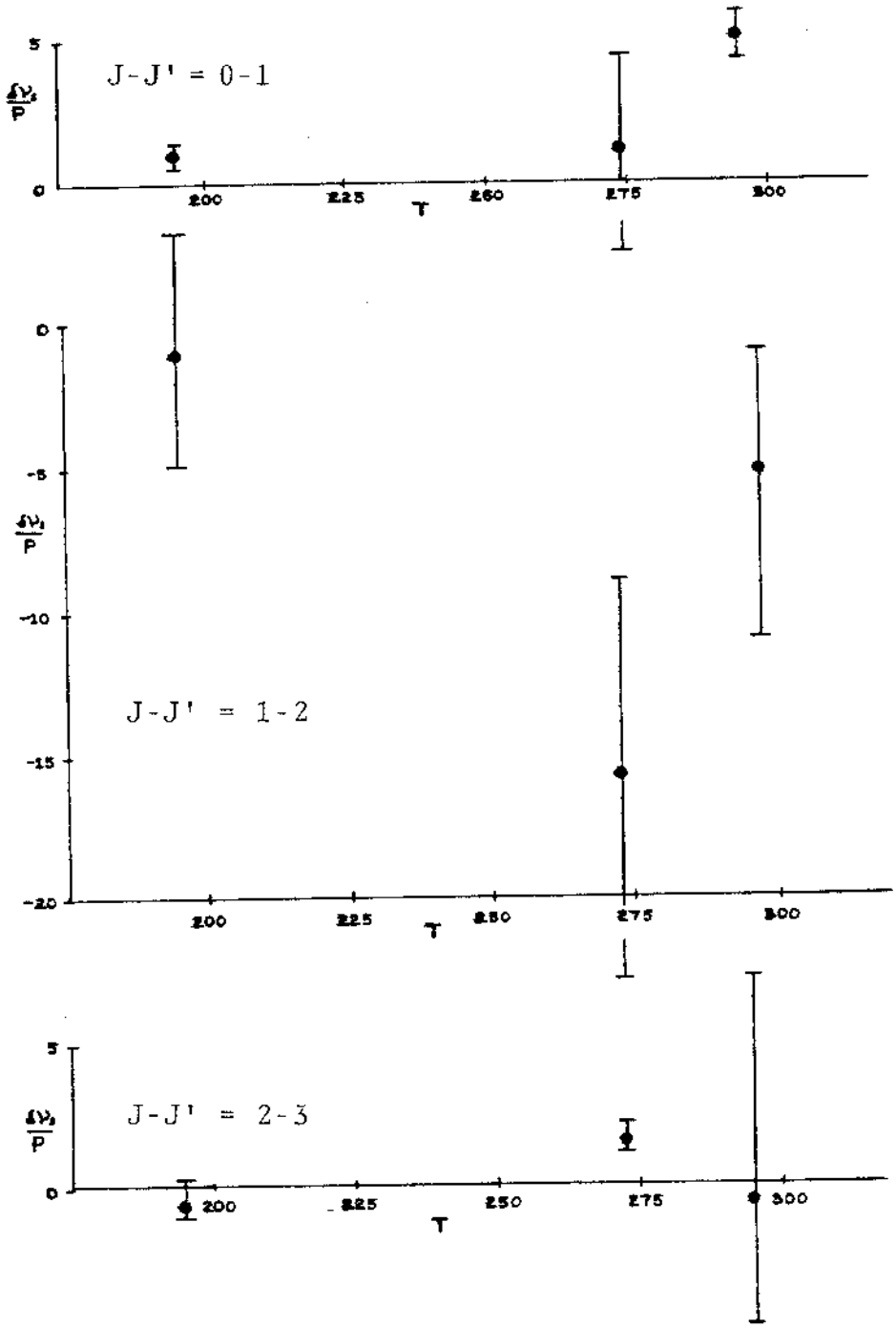


Fig. 16. Temperature dependence of the average line shift parameter.

and the experimental results show good correlation with values reported by other researchers where available.

# CHAPTER VI

# CONCLUSION

It has been seen that a collection of molecules in the gas phase can be probed with microwave radiation, and information can be obtained concerning the molecular interaction mechanisms. When a molecule is approached by another molecule, the energy levels of both molecules are perturbed, and hence the characteristic energy emitted or absorbed by these molecules is changed from its unperturbed value. Examination of the spread in frequency of radiation emitted or absorbed by molecules undergoing collisions gives clues to the nature of the forces acting during the collisions. The method of studying the frequency spread consists of measuring the half width at half-maximum of the absorbtion line that arises from rotational transitions in the molecule. To account for the problem of overlapping spectral lines, a model of overlapping Lorentzian lines broadened by modulation and Doppler effects has been constructed to allow insight into the problem of overlapping hyperfine components of a single envelope. This model has made it possible to extract reliable values of line width parameters for individual hyperfine components.

It has been noted that a need exists for more detailed theoretical work on the subjects of overlapping lines and center frequency shifts. Effective collision diameters for the molecule methyl cyanide have been calculated from the dependence of line half width on pressure. The values provide a reasonable approximation to the range of electrostatic forces of the molecule, or in other words, what another molecule "sees" as the size of the molecule in question.

Measurements of the line shift parameter of methyl cyanide have also been made to determine the effect of collisions that do not induce transitions, but merely cause a phase shift in the emitted or absorbed radiation. These shifts in center frequency of the absorption line were found to be largely masked by standing wave distortion.

It appears that the precision available to the experimenter now exceeds that available from theoretical calculations. In pointing to future investigation, the weakest link in the experimental equipment appears to be the method of determining absolute pressure of the system under consideration, since the electronic measurements have far better reproducibility than is inherently possible with the present pressure-measuring devices. Work has been initiated toward the solution of this problem. These theoretical considerations and pressure-measurement techniques are for future research.

## APPENDIX A
## Quadrupole Interactions

One of the difficulties encountered in the rotational spectrum of $CH_3CN$ lies in the fact that hyperfine components arise within each rotational transition to produce an envelope of spectral lines rather than a single line shape. This effect is discussed below.

If $\Phi$ is the electric potential at the center of mass of the nucleus due to the electron distribution of the molecule, the potential can be expanded in a McLaurin series and the energy of the nuclear charge distribution in an external potential can be written as

$$W = \int d^3x\rho(x,y,z)\{\phi_0 + \left[\left(\frac{\partial\phi}{\partial x}\right)_0 x + \left(\frac{\partial\phi}{\partial y}\right)_0 y + \left(\frac{\partial\phi}{\partial z}\right)_0 z\right]$$

$$+ \frac{1}{2!}\left[\left(\frac{\partial^2\phi}{\partial x^2}\right)_0 x^2 + \left(\frac{\partial^2\phi}{\partial y^2}\right)_0 y^2 + \left(\frac{\partial^2\phi}{\partial z^2}\right)_0 z^2\right]$$

$$+ \left[\left(\frac{\partial^2\phi}{\partial x\partial y}\right)_0 xy + \left(\frac{\partial^2\phi}{\partial y\partial z}\right)_0 yz + \left(\frac{\partial^2\phi}{x\partial z\partial}\right)_0 xz\right] + \ldots$$

$$+ \frac{1}{n!m!p!}\left(\frac{\partial^{n+m+p}}{\partial x^n\partial y^n\partial z^n}\phi\right)_0 x^n y^m z^p + \ldots\} \qquad \text{(A-1)}$$

where $(\frac{\partial\phi}{\partial x})_0$ signifies the derivative of $\phi$ with respect to x, evaluated at the origin. Integrating the first term, we get $Ze\phi$ which is just the energy of a point charge q in a potential $\phi$. It can be shown[39] that the second, third, and

fourth terms integrate to yield the energy of the dipole moment in the x, y, and z directions, respectively, and that these dipole moments are in general zero. The next set of terms is of interest since they comprise the contributions of nuclear quadrupole. The energy of an electric quadrupole in an external potential can be written as [39]

$$W = \int d^3x \rho_{quad.}(\vec{x})\, \phi(\vec{x}) = \int d^3x \frac{1}{6} Q_{ij} \{ \frac{\partial^2}{\partial x_i \partial x_j} \delta(\vec{x}-\vec{x}_0) \} \phi(\vec{x})$$

$$= \int \frac{1}{6} Q_{ij} \delta(\vec{x}-\vec{x}_0) \frac{\partial^2}{\partial x_i \partial x_j} \phi(\vec{x}) = \frac{1}{6} Q_{ij} \left. \frac{\partial^2 \phi(\vec{x})}{\partial x_i \partial x_j} \right|_{\vec{x}=\vec{x}_0}$$

$$= \int -\frac{1}{6} Q_{ij} \frac{\partial E_j(\vec{x}_0)}{\partial x_{j0}} \qquad \text{(A-2)}$$

where $Q_{ij}$ is the $(ij)^{th}$ component of the quadrupole moment tensor, given by [39]

$$Q_{ij} = \int d^3x \rho(\vec{x}) (3x_i x_j - r^2 \delta_{ij}). \qquad \text{(A-3)}$$

We can rotate Q to a normal coordinate frame, that is with z the axis of nuclear spin, so that off-diagonal terms vanish and Q is diagonal. Since Q must be traceless, $(Q_{11} + Q_{22} + Q_{33} = 0)$, we have[39]

$$\int d^3x \rho(\vec{x}) (3x^2 - r^2) = \int d^3x \rho(\vec{x}) (3y^2 - 4^2)$$

$$= \int -\frac{1}{2} d^3x \rho(\vec{x}) (3z^2 - r^2) \qquad \text{(A-4)}$$

so that we can define the nuclear "quadrupole moment" to be[39]

$$Q = \frac{1}{e} \int (\vec{x})(3_z{}^2 - r^2)\,dxdydz. \qquad \text{(A-5)}$$

Expressing the energy in this diagonal system, can be expressed as[39]

$$W_{quad.} = \frac{e}{6} Q\{\frac{\partial^2\phi}{\partial z^2} - \frac{1}{2}\left(\frac{\partial^2\phi}{\partial x^2} + \frac{\partial^2\phi}{\partial y^2}\right)\}. \qquad \text{(A-6)}$$

If the source of $\phi$ is entirely outside the nucleus, we have from Laplace's equation[39]

$$\frac{\partial^2\phi}{\partial x^2} + \frac{\partial^2\phi}{\partial y^2} = - \frac{\partial^2\phi}{\partial z^2}, \qquad \text{(A-7)}$$

so that[39]

$$W_{quad.} = \frac{e}{4} Q\left(\frac{\partial^2\phi}{\partial z^2}\right) . \qquad \text{(A-8)}$$

We should average over all the positions of the electrons and call[39]

$$W_{quad.} = \frac{e}{4} Q\left(\frac{\partial^2\phi}{\partial z^2}\right)_{avg.} \qquad \text{(A-9)}$$

From a quantum mechanical treatment of the problem given by Casimir,[26] we arrive at an expression for the quadrupole interaction energy involving quantum numbers of the rotational states and some measurable constants of the system[26]

$$W_{quad.} = - \frac{eq_m Q\left[\frac{3k^2}{J(J+1)} - 1\right]}{I(2I-1)(2J-1)(2J+3)} (3/4)\{C(C+1) - I(I+1)J(J+1)\} \qquad \text{(A-10)}$$

where $C = F(F+1) - I(I+1) - J(K+1)$. (A-11)

For a nucleus of spin I, there is coupling of the spin with the angular momentum of the molecule, giving rise to another quantum number, F.,

$$\vec{F} = \vec{I} + \vec{J} \text{ or, } F = I + J,\ I + J - 1, \ldots, I - J. \qquad \text{(A-12)}$$

## APPENDIX B

### Derivation of Expression for Energy Stored During a Transition

The probability that a molecule which was in state n at time $t_o-\theta$ has absorbed energy and made a transition to state m by time $t_o$ is given by the squared probability amplitude $a_m^*(t_o)a_m(t_o)$. If $\delta N$ molecules are considered, the number of molecules in state n is proportional to $f_n\delta N$, where $f_n$ is the Boltzmann factor, $\exp(-\hbar\omega_n/kT)$. $\delta N$ may be related to the total number of molecules involved, N, by considering the molecules in the system which had their last collision before time $t_o$ in the interval $t_o-\theta-\delta\theta$ to $t_o-\theta$. If these molecules are $\delta N$ and the mean time between collisions for the system is $\tau$, then,

$$\delta N = \frac{N}{\tau} \exp\left[-\theta/\tau\right] \delta\theta \qquad \text{(B-1)}$$

If $\hbar\omega_{mn}$ is defined to be the energy difference between states m and n, the total energy absorbed by all molecules which emerged from their last collision before time $t_o$ may be written as[23]

$$W_{mn}(t_o) = \int_0^\infty a_m^*(t_o)a_m(t_o)\hbar\omega_{mn} \frac{f_n N}{\tau} \exp(-\theta/\tau)d\theta \ . \qquad \text{(B-2)}$$

A similar expression for the energy emitted by molecules undergoing stimulated emission while making the transition from state m to state n may be found with the same transition probability, but a different state population determined by the Boltzmann factor $f_m = \exp(-\hbar\omega_m/kT)$. The difference in the energy absorbed by molecules in state n and the energy emitted by molecules in state m is the total energy stored by the molecular system when only transitions between states m and n are considered. This net energy may be written as[23]

$$\begin{aligned} W(t_o) &= W_{nm}(t_o) + W_{mn}(t_o) \\ &= \int_0^\infty a_m^*(t_o)a_m(t_o)(\hbar\omega_{mn})^2 \frac{f_n N}{kT\tau} \exp(-\theta/\tau)d\theta, \end{aligned} \qquad \text{(B-3)}$$

where the exponential Boltzmann factor has been expanded in its Taylor series and the approximation has been made that $\hbar\omega_{mn}/kT >> 1$.

# APPENDIX C

## Graphs of Additional Data

In the following pages is the set of figures which represent the complete study of line width parameters.

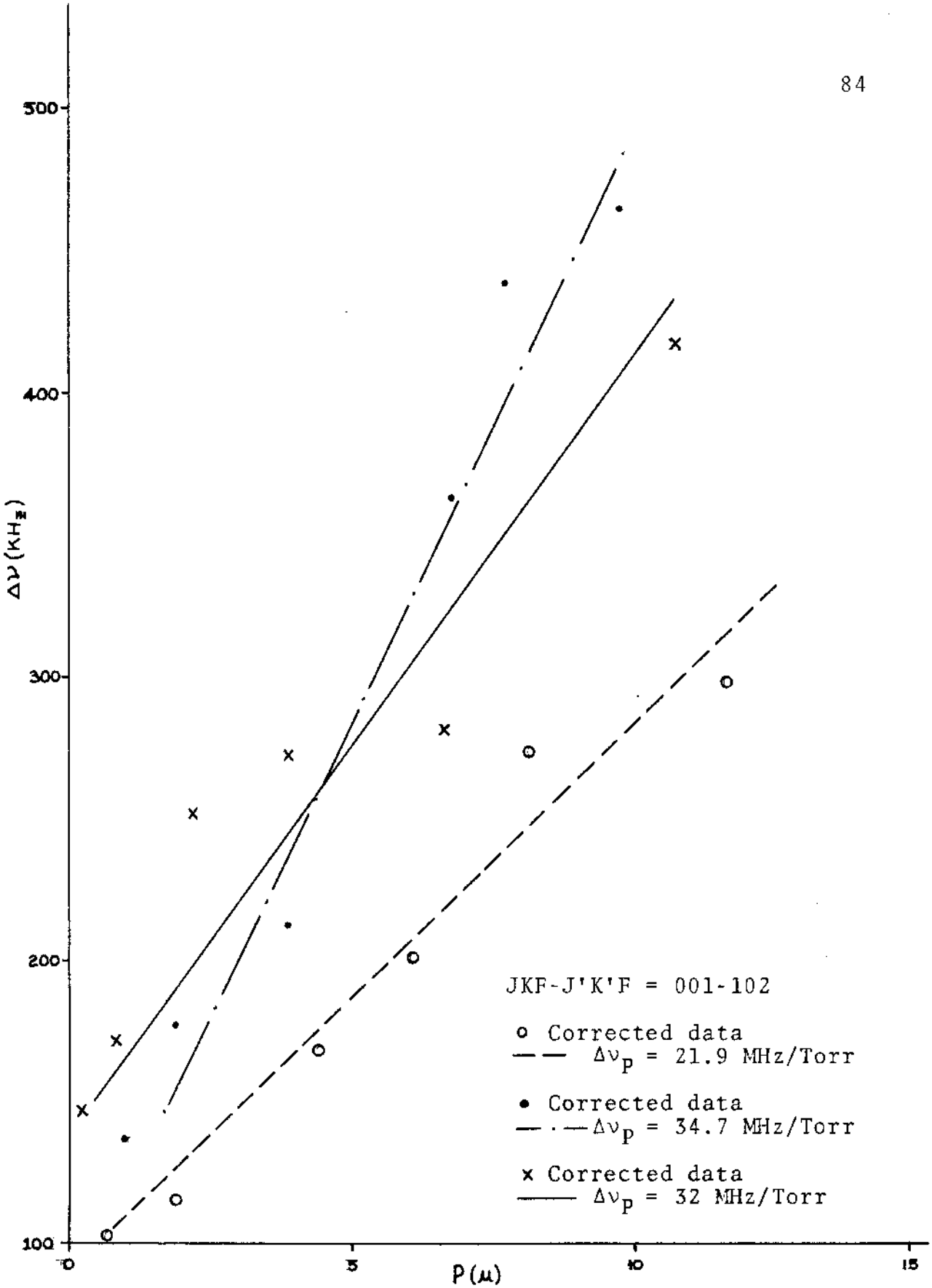


Fig. 17--Experimental data for the line width dependence on pressure for $CH_3CN$ at T = 300 K for the J-J' = 0-1 transition.

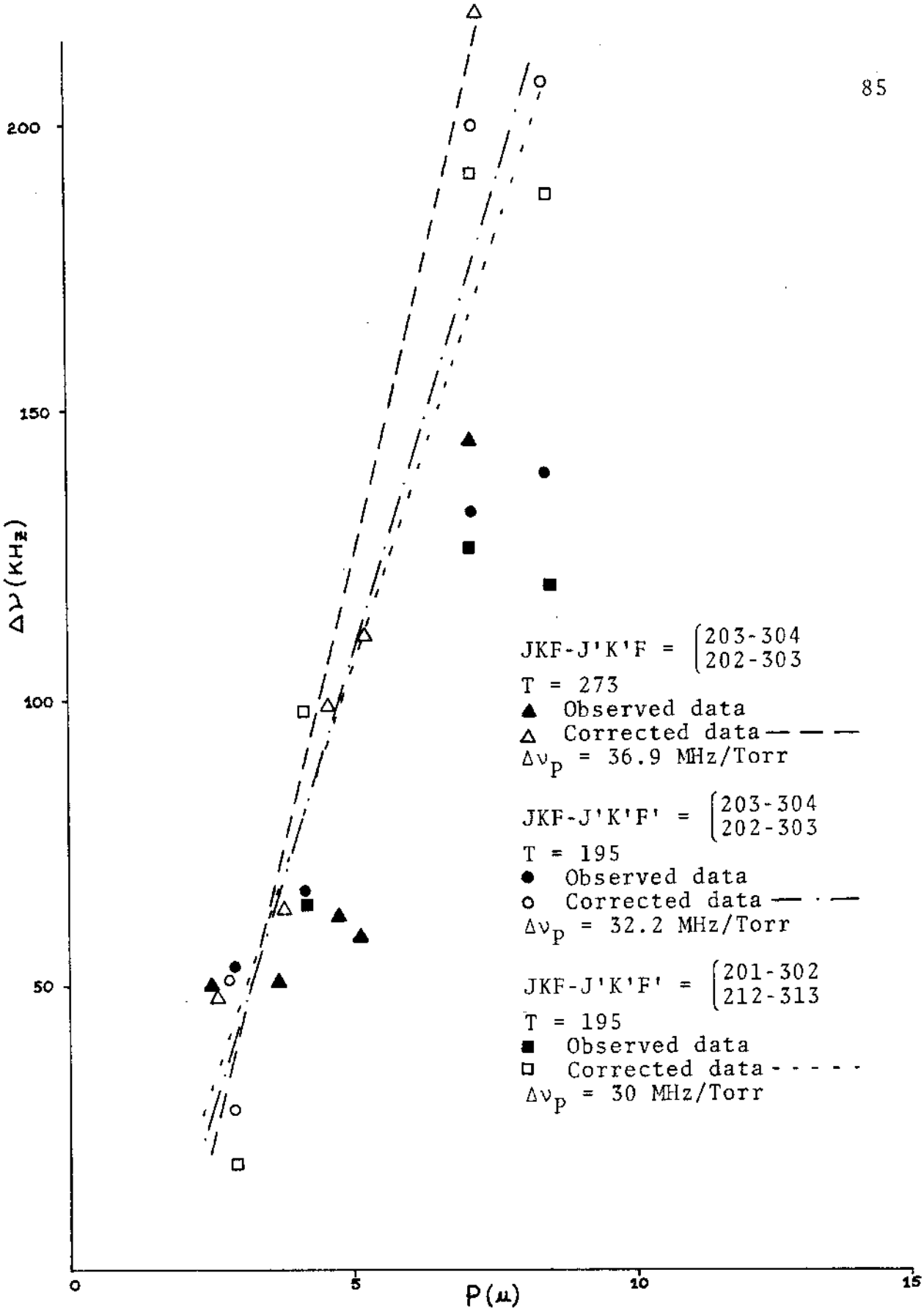


Fig. 18--Experimental data for the line width dependence on pressure for $CH_3CN$ for the J-J' = 2-3 transition.

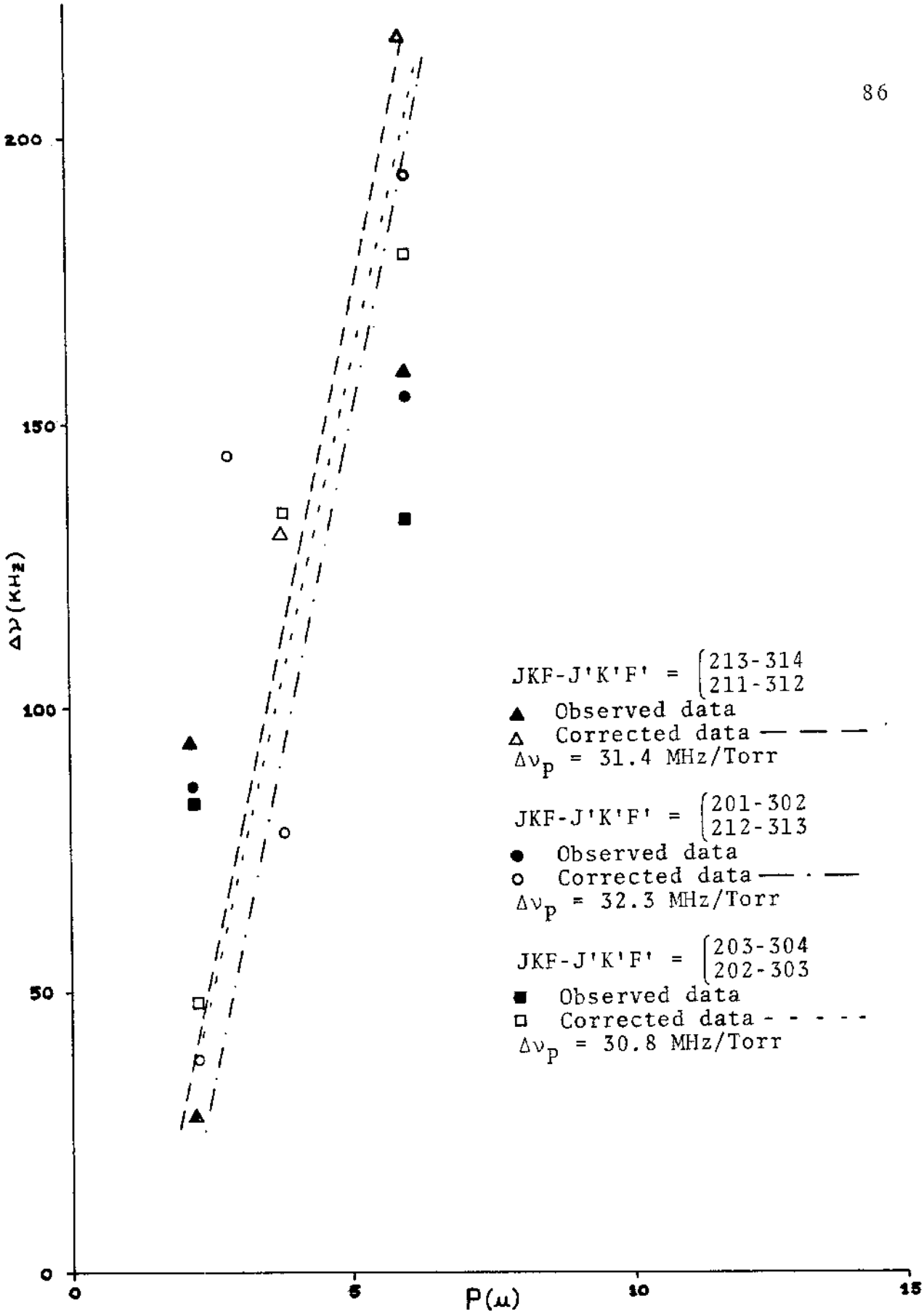


Fig. 19--Experimental data for the line width dependence on pressure for $CH_3CN$ at T = 300K for the J-J' = 2-3 transition.

# APPENDIX D

## Computer Program Listing

In the following pages is a listing of the computer program used in generating the Netterfield line shape which was used to analyze the problem of modulation broadening and overlapping line broadening.

```
      PROGRAM PROFL
      DIMENSION BS(101),BT(101),BX(101)
      COMMON/Q/FNU(242),EK(242),M
      COMMON Q2,DP2,QX,COF1,COF2,UPI,FLAG,C,DLNU,DEL2,QC
      EXTERNAL FT1
      DOUBLE PRECISION CFR1,CFR2,CFR3,CFR4,CFR5,CFR6
      DOUBLE PRECISION QX
      READ(5,10) DF,F1,A1,DUM,M
      READ(5,13) CFR1,CFR2,CFR3,CFR4,CFR5,CFR6
      READ(5,17) CONS1,CONS2,CONS3,CONS4,CONS5,CONS6
      READ(5,18) TP
C     B1 IS THE MOLECULAR MASS, TP IS THE ABS. TEMPERATURE.
      DLNU = 10.
      B1 = 6.84700 E-26
      C = 3.00000 E+8
      BC = 1.3800 E-23
      PI = 3.14159
      COF2 = 8.*PI**3
      UPI = 2.*PI/COF2
      K = 0
      X = DF/F1
      WRITE(6,14) CFR1,CONS1,CFR2,CONS2,CFR3,CONS3,CFR4,
     1,CONS4,CFR5,CONS5-CFR6,CONS6
      WRITE(6,10) DF,F1,A1,DUM,M
      WRITE(6,112) DLNU
  401 CONTINUE
      DO 1 N = 1,20
      NA = N-10
      IF(NA.GE.0) GO TO 2
      NP = IABS(NA)
      CALL BESJ(X,NP,BN,D,TER)
      BS(N) = BN*(-1.)**NP
      GO TO 3
    2 CALL BESJ(X,NA,BN,D,TER)
      BS(N) = BN
    3 CONTINUE
      IF(IER.EQ.4) GO TO 30
      IF(IFR.EQ.4) GO TO 30
    1 CONTINUE
      NB = 19-K
      DO 4 N=1,NB
      BX(N) = BS(N)*BS(N+K)
```

```
 4 CONTINUE
   WRITE(6,22)(BS(N),BX(N),N=1,NB)
   DO 70 J = 1,10
   DUM = -275.
   DEL2 = DLNU*DLNU
   Q3 = FLOAT(K)
   DP2 = Q3*F1
   COF1 = B1/(2.*BC*TP)
   DO 6 I = 1,M
   QX = CFR1 + DUM
   FNU(I) = QX-36790000.
   QC = QX/(C*SQRT(COF1))
   SUM1 = 0.0
   SUM2 = 0.0
   SUM3 = 0.0
   SUM4 = 0.0
   SUM5 = 0.0
   SUM6 = 0.0
   DO 7 N=1,NB
   NA = N-9
   Q2 = F1*FLOAT(NA)
   FLAG = 0.
   CALL QH10(FT1,P1,CFR1)
   CALL QH10(FT1,P3,CFR2)
   CALL QH10(FT1,P5,CFR3)
   FLAG = 1.
   CALL QH10(FT1,P2,CFR1)
   CALL QH10(FT1,P4,CFR2)
   CALL QH10(FT1,P6,CFR3)
   SUM1 = SUM1 + P1*BX(N)
   SUM2 = SUM2 + P2*BX(N)
   SUM3 = SUM3 + P3*BX(N)
   SUM4 = Sum4 + P4*BX(N)
   SUM5 = SUM5 + P5*BX(N)
   SUM6 = SUM6 + P6*BX(N)
 7 CONTINUE
   E1 = CONS1*SQRT((SUM1)**2+(SUM2)**2)
   E2 = CONS2*SQRT((Sum3)**2+(SUM4)**2)
   E3 = CONS3*SQRT((SUM5)**2+(SUM6)**2)
   EK(I) = E1+E2+E3
   DUM = DUM + A1
 6 CONTINUE
   GO TO 9
30 WRITE (6,110)
 9 CONTINUE
   CALL DRAWAR (20.0,0.0)
   DLNU = DLNU + 10.
```

```
 70 CONTINUE
    CALL LOUT(20.0,0.0)
 10 FORMAT(4F10.1,I5)
 13 FORMAT (4F15.5)
 14 FORMAT (1H,E20.12,F10.4)
 17 FORMAT (6F10.5)
 18 FORMAT (F10.3)
 22 FORMAT (1H,2E20.12)
110 FORMAT (29H ORDER OF BESSEL FN TOO LARGE)
112 FORMAT (13H       DELNU = ,F7.2)
    STOP
    END


    FUNCTION FT1(CFR,X)
    COMMON Q2,DP2,QX,COF1,COF2,UPI,FLAG,C,DLNU,DEL2,QC
    DOUBLE PRECISION QX,CFR,X
    FT1 = 0.0
    DM1 = QX - CFR + Q2
    DM2 = DP2+DM1
    DM3 = X*QC
    TDM1 = (DM1+DM3)*(DM1+DM3)
    TDM2 = (DM2+DM3)*(DM2+DM3)
    IF(FLAG.EQ.1.) GO TO 2
    TNUM = (2.*DLNU+(TDM1+TDM2)/DLNU)*QC
    GO TO 3
  2 TNUM = (TDM1*TDM2-UPI)*DP2*QC
  3 CONTINUE
    TDEN = COF2*(DEL2+TDM1)*(DEL2+TDM2)
    IF(TDEN.EQ.0.0) GO TO 1
    FT1 = TNUM/TDEN
  1 RETURN
    END
```

```
C       COMPUTES THE J BESSEL FUNCTION FOR A GIVEN ARGUMENT
       1AND ORDER
C       DESCRIPTION OF PARAMETERS
C         X - THE ARGUMENT OF THE BESSEL FN
C         N - THE ORDER
C         BJ -THE  RESULTANT BESSEL
C         D - REQUIRED ACCURACY
C        IER -ERROR  CODE
C        IER -IER+0 NO ERROR
C       IER = 2 x TS NEG OR ZERO
C       IER = 3 DESIRED ACCURACY NOT OBTAINED
C       IER = 4 RANGE OF N COMPARED TO X INCORRECT
C             IFR=1 N IS NEG
C        REMARKS
C            N MUST BE .GE. ZERO BUT .LT.
C                 20 + 10*X-X**2/3 FOR X .LE.15
C                 90 + X/2         FOR X .GT.15
C        METHOD OF H. GOLDSTEIN AND R.M.THALER
        SUBROUTINE BESJ (X,N,BJ,D,TER)
        BJ=0.0
        IF(N)10,20,20
     10 IER=1
        RETURN
     20 IF(X)30,30,31
     30 IER=2
        RETURN
     31 IF(X-15.)32,32,34
     32 NTEST=20.+10.*X-X**2/3
        GO TO 36
     34 NTEST=90.+X/2
     36 IF(N=NTEST)40,38,38
     38 IER=4
        RETURN
     40 IER=0
        N1=N+1
        BPREV=.0
C       COMPUTE STARTING VALUE OF N
        IF(X=5.)50,60,60
     50 MA=X+6.
        GO TO 70
     60 MA=1.4*X+60./X
     70 MB=N+IFIX(X)/4+2
        IF(MA.GT.MB) GO TO 5
        MZERO = MB
        GO TO 6
      5 MZERO = MA
      6 CONTINUE
C       SET UPPER LIMIT OF N
        MMAX=NTEST
```

```
100 DO 190 M=MZERO,MMAX,3
    SET F(M),F(M-1)
    FM1=1.0E-28
    FM=.0
    ALPHA=.0
    IF (M-(M/2)*2)120,110,120
110 JT=-1
    GO TO 130
120 JT=1
130 M2=M-2
    DO 160 K=1,M2
    MK=M-K
    BMK=2.*FLOAT(MK)*FM1/X-FM
    FM=FM1
    FM1=BMK
    IF(MK-N-1)150,140,150
140 BJ = BMK
150 JT=-JT
    S=1+JT
160 ALPHA=ALPHA+BMK*5
    BMK=2.*FM1/X-FM
    IF(N)180,170,180
170 BJ=BMK
180 ALPHA=ALPHA+BMK
    BJ=BJ/ALPHA
    IF(ABS(BJ=BPREV)-ABS(D*BJ))200,200,190
190 BPREV=BJ
    IER=3
200 RETURN
    END


    SUBROUTINEQH10(FCT,Y,CFR)
    DOUBLE PRECISION CFR,X,Z
    X = 2.020183
    Z = -X
    Y = .01995324*(FCT(CFR,X)+FCT(CFR,Z))
    X = .9585725
    Z = -X
    Y = Y + .3936193*(FCT(CFR,X)+FCT(CFR,Z))
    X = 0.0
    Y = Y + .9453087*(FCT(CFR,X))
    RETURN
    END
```

```
SUBROUTINE DRAWAR(G,H)
DIMENSION IBUF(4000)
COMMON/Q/C(242),D(242),N
L = N
M = N+1
O = N+2
CALL PLOTS(IBUF,4000,6)
CALL FACTOR(.25)
CALL PLOT(G,H,-3)
CALL SCALE(C,18.0,L,1)
CALL SCALE(D,13.0,L,1)
CALL AXIS(0.0,0.0,11HOMEGA (MHZ),-11,18.,0.0,C(M),C(O))
CALL AXIS(0.0,0.0,7HPROFILE,+7,13.,90.0,D(M),D(O))
CALL LINE (C,D,L,1,0,0)
RETURN
ENTRY LOUT(G,H)
CALL PLOT(20.,0.0,999)
RETURN
END
```

## REFERENCES


1. H. A. Lorentz, The Theory of Electrons, (Dover,New York, 1909), note 57.

2. P. Debye, Polar Molecules, (Chemical Catalog Company, Inc., New York).

3. V. F. Weisskopf, Phys. Zeits. 34, 1 (1933).

4. W. Gordy, Rev. Mod. Phys 20, 668 (1948).

5. J. H. Van Vleck and V. F. Weisskopf, Rev. Mod. Phys. 17, 227 (1945).

6. P. W. Anderson, Phys. Rev. 26, 647, (1949).

7. J. S. Murphy and J. E. Boggs, J. Chem. Phys. 47, 691 (1967).

8. C. J. Tsao and B. Curnutte, J. Quan. Spectry. Radiative Transfer 2, 41 (1962).

9. B. S. Frost, J. Phys. B; Atom. Mol. Phys. 9, 1041 (1976).

10. E. Herbst and W. Klemperer, Phys. Today, 7, 35 (1976)

11. A. C. Venkatachar and J. A. Roberts, J. Chem. Phys. 62, 3364 (1975).

12. D. V. Rogers and J. A. Roberts, J. Mol. Spectrosc. 46, 200 (1973).

13. J. A. Roberts, J. Phys. Chem. 74, 1923 (1970).

14. C. H. Townes and A. L. Shawlow, Microwave Spectroscopy, (McGraw-Hill, New York, 1955).

15. W. H. Ghosh, R. Trombarulo, and W. Gordy, Phys. Rev. 87, 172A (1952).

16. D. K. Coles, W. E. Good, and P. H. Hughes, Phys. Rev. 79, 224A (1950).

17. D. Boucher, J. Burie, J. Demaison, A. Dubrulle, J. Legrand, B. Segard, J. Mol. Spectrosc. 64, 290 (1977).

18. J. A. Roberts, Rev. Sci. Instr. 45,

19. Townes and Schawlow, Ibid., p. 336.

20. V. F. Weisskopf and E. H. Wigner, Zeits. Phys. 63, 54 (1930).

21. A. Karplus, Phys. Rev. 73, 1027

22. E. A. Rinehart, R. H. Kleen, and C. C. Lin, J. Mol. Spectrosc. 5, 478

23. R. P. Netterfield, R. W. Parsons, and J. A. Roberts, J. Phys. B: Atom. Molec. Phys. 5, 146 (1972).

24. I. C. Story, V. I. Metchnik, and R. W. Parsons, J. Phys. B: Atom. Molec. Phys. 4, 593 (1971).

25. S. Goldman, Frequency Analysis, Modulation and Noise, (McGraw-Hill, New York, 1948).

26. Townes and Schawlow, Ibid., p. 78.

27. H. B. G. Casimir, On the Interaction Between Atomic Nuclei and Electrons, (W. H. Freeman and Company, San Francisco, 1963).

28. Townes and Schawlow, Ibid., p. 499.

29. Townes and Schawlow, Ibid., p. 74.

30. H. Kuhn and F. London, Phil. Mag. 18, 983 (1934).

31. H. Margenau, Phys. Rev. 82, 156 (1951).

32. G. Birnbaum, J. Chem. Phys. 46, 2455 (1967).

33. Krisnaji and S. L. Srivastiva, J. Chem. Phys. 41, 2266 (1964).

34. Krishnaji and S. L. Srivastiva, J. Chem. Phys. 42, 1456 (1965).

35. I. R. Dagg, J. A. Roberts, and R. W. Parsons, J. Mol. Spectrosc. 63, 241 (1976).

36. Townes and Schawlow, Ibid., p. 414.

37. G. P. Srivastiva, H. O. Guatam, and A. Kumar, J. Phys. B: Atom. Mol. Phys. 6, 743 (1973).

38. J. A. Roberts and R. W. Parsons, J. Mol. Spectrosc. 18, 412 (1966).

39. J. H. Jeans, Dynamical Theory of Gases, (Cambridge Univ. Press, New York, 1921) 3rd ed., pp. 37, 352.

40. Townes and Schawlow, Ibid., p. 133.